Oxidative Steam Reforming of Raw Bio-Oil over Supported and Bulk Ni Catalysts for Hydrogen Production

Aitor Arandia [1], Aingeru Remiro [1],* [iD]**, Verónica García [2], Pedro Castaño [1]** [iD]**, Javier Bilbao [1] and Ana G. Gayubo [1]**

[1] Chemical Engineering Department, University of the Basque Country, P.O. Box 644, 48080 Bilbao, Spain; aitor.arandia@ehu.eus (A.A.); pedro.castano@ehu.eus (P.C.); javier.bilbaoe@ehu.eus (J.B.); anaguadalupe.gayubo@ehu.eus (A.G.G.)

[2] Grupo de Investigación en Química Estructural GIQUE, Universidad Industrial de Santander, 680002 Bucaramanga, Colombia; vgarojas@uis.edu.co

* Correspondence: aingeru.remiro@ehu.eus; Tel.: +34-946-015-361; Fax: +34-946-013-500

Abstract: Several Ni catalysts of supported (on La_2O_3-αAl_2O_3, CeO_2, and CeO_2-ZrO_2) or bulk types (Ni-La perovskites and $NiAl_2O_4$ spinel) have been tested in the oxidative steam reforming (OSR) of raw bio-oil, and special attention has been paid to the catalysts' regenerability by means of studies on reaction-regeneration cycles. The experimental set-up consists of two units in series, for the separation of pyrolytic lignin in the first step (at 500 °C) and the on line OSR of the remaining oxygenates in a fluidized bed reactor at 700 °C. The spent catalysts have been characterized by N_2 adsorption-desorption, X-ray diffraction and temperature programmed reduction, and temperature programmed oxidation (TPO). The results reveal that among the supported catalysts, the best balance between activity-H_2 selectivity-stability corresponds to Ni/La_2O_3-αAl_2O_3, due to its smaller Ni^0 particle size. Additionally, it is more selective to H_2 than perovskite catalysts and more stable than both perovskites and the spinel catalyst. However, the activity of the bulk $NiAl_2O_4$ spinel catalyst can be completely recovered after regeneration by coke combustion at 850 °C because the spinel structure is completely recovered, which facilitates the dispersion of Ni in the reduction step prior to reaction. Consequently, this catalyst is suitable for the OSR at a higher scale in reaction-regeneration cycles.
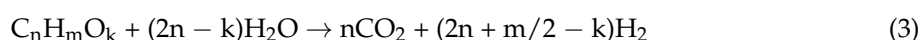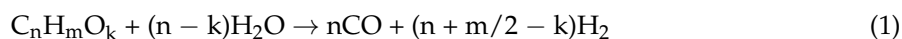
Keywords: bio-oil; Ni catalyst; oxidative steam reforming; H_2 production; deactivation; regeneration
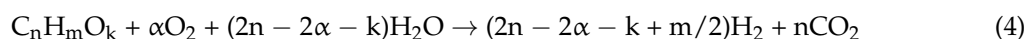
1. Introduction

The world energy industrial sector is in a technological transition stage from the traditional processes for obtaining energy from non-renewable sources (oil, coal, natural gas) towards new sustainable and environmentally friendly processes, with the objective of attaining in the middle-term a neutral balance of greenhouse gases emissions. In this scenario, the development of sustainable H_2 production technologies plays a significant role [1–3], with a special interest in the routes from lignocellulosic biomass [4,5] due to its high availability and whose valorisation does not interfere in the feeding chain. Among these routes from biomass, great attention is paid to the H_2 production by steam reforming (SR) of bio-oil, the liquid product from the pyrolysis of lignocellulosic biomass [6–8]. Bio-oil can be obtained in a decentralised way by means of fast pyrolysis, with simple and environmentally friendly technologies, which are in industrialisation development [9]. In spite of its renewable nature, the low content of S and N, and neutral CO_2 balance for combustion, bio-oil is not suitable for direct use as a fuel due to its instability and properties (such as high water and oxygen

content, acidity, corrosiveness and low viscosity). Consequently, several processes have been proposed for stabilizing, conditioning and up-grading bio-oil in order to convert it into platform chemicals (olefins and BTX), liquid fuels or H_2 [10–12]. Thus, the bio-oil produced in decentralised pyrolysis units can be subsequently transported to a centralized unit for H_2 production. This transport is more economical than that of the biomass, due to the higher density of bio-oil [13]. Compared to other routes for valorising bio-oil, steam reforming has the additional advantage that it does not require water separation.

The SR of bio-oil is a highly endothermic reaction [6,8,14] that follows the general stoichiometry of oxygenates reforming, Equation (1), and considering the water gas shift reaction, Equation (2), the complete stoichiometry of this overall reaction is given by Equation (3).

$$C_nH_mO_k + (n - k)H_2O \rightarrow nCO + (n + m/2 - k)H_2 \tag{1}$$

$$CO + H_2O \leftrightarrow CO_2 + H_2 \tag{2}$$

$$C_nH_mO_k + (2n - k)H_2O \rightarrow nCO_2 + (2n + m/2 - k)H_2 \tag{3}$$

The addition of oxygen together with water promotes the partial oxidation of some compounds in the reaction medium, thus decreasing the energy requirements for the endothermic steam reforming reaction, although to the expense of a lower H_2 production. This reaction is known as oxidative steam reforming (OSR) (Equation (4)) and with a suitable ratio of O_2/steam/carbon in the feed, a thermoneutral regime can be achieved [14,15].

$$C_nH_mO_k + \alpha O_2 + (2n - 2\alpha - k)H_2O \rightarrow (2n - 2\alpha - k + m/2)H_2 + nCO_2 \tag{4}$$

In addition to the reforming reaction, secondary reactions (cracking/decomposition methanation, Boudouard reaction) can also take place, thus decreasing the potential H_2 production.

Due to the difficulty in handling bio-oil because of its complex nature (a mixture with more than 300 oxygenated compounds belonging to different families), the SR and OSR has been extensively studied with pure oxygenates, mainly ethanol [16–18], and OSR experimental studies with raw bio-oil have been scarcely addressed in the literature [19,20]. Remiro et al. [15] reported the better performance in the OSR of raw bio-oil at 700 °C of a Rh/CeO_2-ZrO_2 catalyst over a supported Ni/La_2O_3-αAl_2O_3 catalyst due to the higher activity and stability of the former. The higher stability of the Rh catalyst was attributed to a lower encapsulating coke deposition and much lower metal sintering compared to the Ni catalyst. Nevertheless, in the conditions needed for attaining high bio-oil conversion (above 600 °C), the Rh/CeO_2-ZrO_2 catalyst suffers structural changes, both in the Rh species and in the support (aging) [21], which is a handicap for the total recovery of its activity subsequent to regeneration by total coke removal by combustion with air [22]. This fact, together with the high cost of the Rh-based catalyst, advice us to continue searching for cheaper catalysts with suitable performance in the OSR of raw bio-oil.

With this background, the objective of this work has been the selection of a suitable catalyst for the OSR of raw bio-oil, based on the best compromise between activity, H_2 selectivity, and stability in the selected reaction conditions, but paying special attention to its capacity for activity recovery after regeneration, as this is a key factor for the industrial viability of the process which has been scarcely studied in the literature. For that purpose, Ni-based catalysts have been selected due to their good performance for reforming of oxygenated compounds and lower cost compared to noble metal catalysts. The catalysts studied include (i) supported catalysts, prepared in the laboratory with different supports (La_2O_3-Al_2O_3, CeO_2, CeO_2-ZrO_2) and a commercial catalyst (G90) for comparison. The variety of studied supports has allowed analysing the relevance of the metal-support interaction on the Ni catalyst properties and, consequently, on their catalytic behaviour, and; (ii) bulk catalysts, of Ni-La perovskite-type ($LaNiO_3$ and L_2NiO_4) and Ni-Al spinel type ($NiAl_2O_4$). The estate of Ni and the metal-support interaction will affect the ability for the adsorption of the chemical compounds in the

reaction medium and, consequently, their reactivity. Thus, Politano and Chiarello [23] have proven the relevance of the co-adsorption of other compounds in the reaction medium on the adsorption of CO on Ni sites, with the formation of intermediate COH with the adsorbed H. This complex behaviour of Ni sites makes the interpretation of the results difficult. The experimental runs were carried out in an experimental device with two units in series (thermal step and catalytic step, the latter in fluidized bed reactor), whose adequacy for SR and OSR of aqueous and raw bio-oil has been previously proven, as it minimizes operating problems (such as plugging of reactor piping) as well as catalyst deactivation in the reforming step [15,21,22,24–27]. The properties of the catalysts have been determined with different techniques (N_2 adsorption-desorption, Temperature Programmed Reduction (TPR), X-ray Diffraction (XRD)), in order to explain the differences in the kinetic behaviour of the catalysts. The activity recovery has been studied by means of reaction-regeneration cycles, with regeneration involving combustion with air for complete coke removal.

2. Results

2.1. Catalyst Properties

2.1.1. Physical Properties (N_2 Adsorption-Desorption)

Tables 1 and 2 show the physical properties (BET Surface, pore volume, and mean pore diameter) of the supported and bulk catalysts, respectively, obtained from the corresponding N_2 adsorption-desorption isotherms. The differences in the physical properties of the supported catalysts (Table 1) can be attributed to the differences in their corresponding support, with the BET surface of CeO_2 support (Ce) (191.8 m^2 g^{-1}) being much higher than that of La_2O_3-αAl_2O_3 (LaAl) and the CeO_2-ZrO_2 (CeZr) supports (41.4 m^2 g^{-1} and 47.5 m^2 g^{-1}, respectively). Consequently, the Ni/Ce catalyst has the higher porosity, with the values of BET Surface, pore volume, and pore diameter (159.2 m^2 g^{-1}, 0.312 cm^3 g^{-1} and 8.2 nm, respectively) lower than the Ce support due to the partial blockage by Ni [28]. The decrease in the support accessibility after impregnation is also observed for the Ni catalysts supported on CeZr and on LaAl, in accordance with the literature [29–31]. For Ni/CeZr catalysts, an increase in the Ni content involves a decrease in surface area and pore volume, but the mean pore diameter increases slightly compared to the support due to the blockage of the pores of lower diameter. The Ni commercial catalyst, G90, has the lower specific surface area and pore volume among the studied supported catalysts.

Table 1. The physical properties of the supports, of the synthetized supported catalysts, and of the commercial G90 catalyst.

Catalyst Supports	S_{BET}, m^2 g^{-1}	V_{pore}, cm^3 g^{-1}	d_{pore}, nm
αAl_2O_3 (Al)	50.0	0.205	8.2
La_2O_3-αAl_2O_3 (LaAl)	41.4	0.154	14.5
CeO_2 (Ce)	191.8	0.417	8.8
CeO_2-ZrO_2 (CeZr)	47.6	0.121	7.9
Synthetized Catalysts			
Ni/LaAl	37.6	0.145	14.6
Ni/Ce	159.2	0.312	8.2
5Ni/CeZr	31.6	0.133	10.2
15Ni/CeZr	23.2	0.116	10.4
Commercial Catalyst			
G90	19.0	0.041	12.2

The low values of BET surface area observed in Table 2 for the Ni-La perovskites are characteristic for these materials with low porosity [32,33]. Nevertheless, there are differences between the two

types of perovskites due to the meso-macroporosity of LaNiO$_3$ catalyst, so that the meso-macropore volume of this catalyst (0.068 cm^3 g^{-1}, calculated as the difference between total pore volume and that of micropore) is significantly higher than that of La$_2$NiO$_4$ catalyst (0.012 cm^3 g^{-1}). The BET surface area of the Ni-Al spinel type catalyst is significantly higher than those of the perovskite-type, and it is also noticeably higher than that of supported catalysts, except Ni/Ce.

Table 2. The physical properties of the synthetized bulk catalysts of Ni-La perovskite-type and Ni-Al spinel type.

Catalyst	S_{BET}, m^2 g^{-1}	V_{pore}, cm^3 g^{-1}	d_{pore}, nm
LaNiO$_3$	9.2	0.068	29.5
La$_2$NiO$_4$	7.3	0.012	6.8
NiAl$_2$O$_4$	96.8	0.120	5.0

2.1.2. Catalyst Reducibility (Temperature Programmed Reduction (TPR))

Figures 1 and 2 show the TPR profiles of the supported and bulk catalysts, respectively. From these profiles, the reduction temperature for each catalyst has been selected (Table 4 in Section 4) in order to obtain the metal active species (Ni^0).

The TPR profiles of the Ni supported catalysts differ depending on the Ni content and on the support (Figure 1), Ni/LaAl and G90 being those requiring a higher temperature for the reduction of all the oxidized metal species. These results give evidence of the important role of the support and the metal-support interaction on the metal reducibility, so that the Ni-Al$_2$O$_3$ interactions are stronger than the interactions of Ni with CeO$_2$ and/or ZrO$_2$ oxides [34,35].
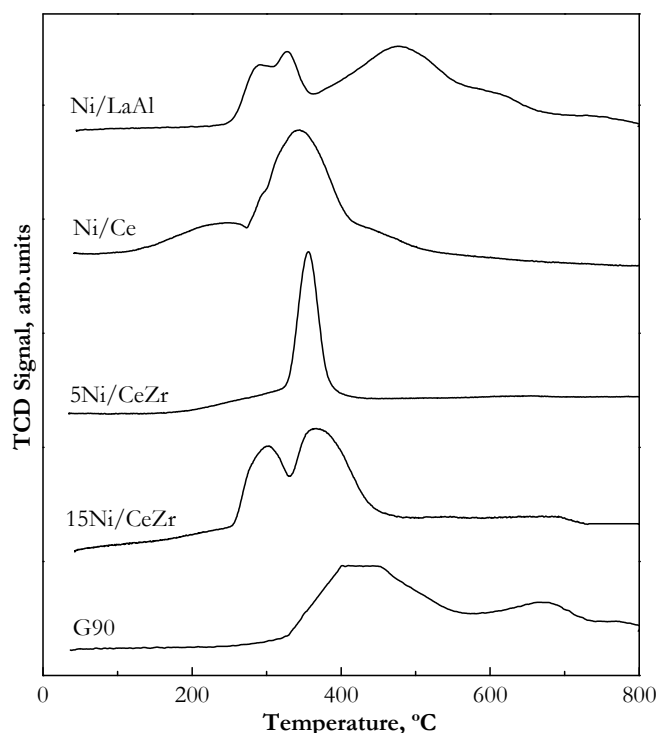

Figure 1. The TPR profiles for the Ni supported catalysts.

Two wide and asymmetric reduction domains are observed for Ni/LaAl catalyst: the reduction to Ni^0 of surface NiO with low interaction with the support takes place in the 250–370 °C range, whereas the band between 370–700 °C corresponds to the reduction to Ni^0 of well dispersed NiO$_x$ species,

probably of an amorphous nature and with high interaction with the support [25]. A reduction peak of low intensity is also observed above 700 °C for the Ni/LaAl catalyst that corresponds to the reduction to Ni^0 of the Ni^{2+} in the spinel phase ($NiAl_2O_4$), whose low intensity is explained by its low calcination temperature (550 °C) because the formation of the spinel requires higher temperatures [25,36]. The commercial catalyst G90 has the main reduction peak with a maximum near 420 °C, attributed to the reduction of NiO with a slight interaction with the αAl_2O_3 support, and a peak near 680 °C probably related to the reduction of Ni^{2+} in the $NiAl_2O_4$ phase, according to the composition given by the provider (*Sud-Chemie*). The Ni/Ce catalyst has two reduction peaks, a minority and wide peak below 250 °C and a main peak in the 250–400 °C range, which correspond to the reduction of the NiO species with different interaction strengths with CeO_2 support [37]. Moreover, the possible reduction of the CeO_2 support around 400 °C should be also taken into account, and this reduction peak can overlap the NiO reduction peak as a consequence of the "*spillover*" phenomena [38,39]. The reduction peak with a maximum at 360 °C for Ni catalysts supported on CeO_2-ZrO_2 corresponds to the reduction of NiO interacting with the support. In the catalyst with higher Ni content (15Ni/CeZr), there is another reduction peak at lower temperature (with a maximum below 300 °C), that can be attributed to the reduction of free NiO species or with weak metal-support interaction [40,41], probably due to the high metal content in the catalyst.

In the Ni-La perovskite-type catalysts, two well-differenced reduction bands are observed (Figure 2), that shift towards higher temperature for the La_2NiO_4 catalyst, which evidences a higher interaction between Ni and La_2O_3 compared to the $LaNiO_3$ catalyst [42]. For the latter, the two reduction bands, with maximum at 280 and 420 °C, correspond to the reduction of the $LaNiO_3$ precursor in two consecutive steps: firstly, the reduction of Ni^{3+} species to Ni^{2+} takes place, thus forming $La_2Ni_2O_5$, which is reduced in the second step at higher temperature to form Ni^0 and La_2O_3 [43–45]. Nevertheless, there is no agreement in the literature concerning the assignment of reduction peaks for the La_2NiO_4 catalyst. Thus, some authors attribute the first peak to the reduction of Ni^{3+} to Ni^{2+} and the second peak to the reduction of Ni^{2+} to Ni^0 [46,47], but others assume that firstly there is a reduction of the excess oxygen in the $La_2NiO_{4+\delta}$ phase, and that the reduction of the resulting La_2NiO_4 phase takes place in one step, near 600 °C [48,49].
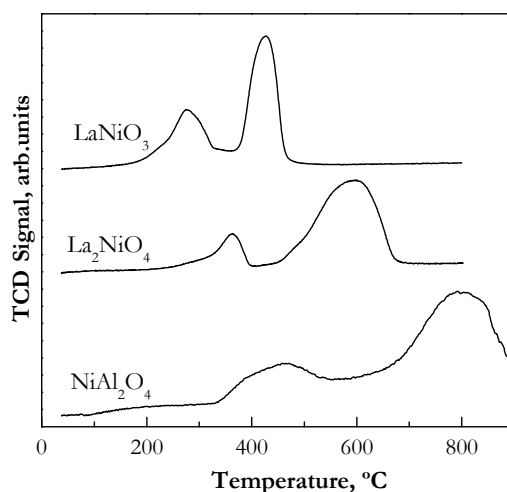

Figure 2. The TPR profiles for the bulk catalysts of Ni-La perovskite and Ni-Al spinel type.

The $NiAl_2O_4$ spinel catalyst has the main reduction peak with a maximum at 800 °C in Figure 2, corresponding to the reduction of Ni^{+2} ions incorporated in the spinel structure, which require high temperatures for breaking the strong bonds [25,50]. The presence of a smaller band with a maximum near 450 °C, corresponding to the reduction to Ni^0 of the NiO with a high interaction with the support, but not being part of the spinel structure, can be due to the use of an excess of Ni or defect of Al in the

synthesis of this catalyst. It could be also attributed to the difficulty of the auto-combustion method for attaining a complete reaction between NiO and Al_2O_3 so that Ni is not completely incorporated in the $NiAl_2O_4$ spinel structure.

2.1.3. Crystalline Structure (X-ray Diffraction (XRD))

Figure 3 shows the X-ray diffractograms for the supported catalysts prior and after reduction (fresh or reduced, respectively), whereas those corresponding to the bulk catalysts are shown in Figure 4. Up to five phases are observed for the Ni/LaAl catalyst, depending on the oxidation state of the sample (Figure 3). Al_2O_3, $NiAl_2O_4$, and $LaAlO_3$ phases are observed in both states (oxidized and reduced), whereas NiO is only observed in the oxidized simple and Ni^0 is only present in the reduced sample. The small fraction of $NiAl_2O_4$ identified in this catalyst (whose formation is incipient in the calcination at 550 °C [25]) is coherent with the small shoulder above 700 °C observed in the TPR profile of this catalyst (Figure 1). This oxidized species remains in the reduced simple because its reduction to Ni^0 requires a temperature above 700 °C.
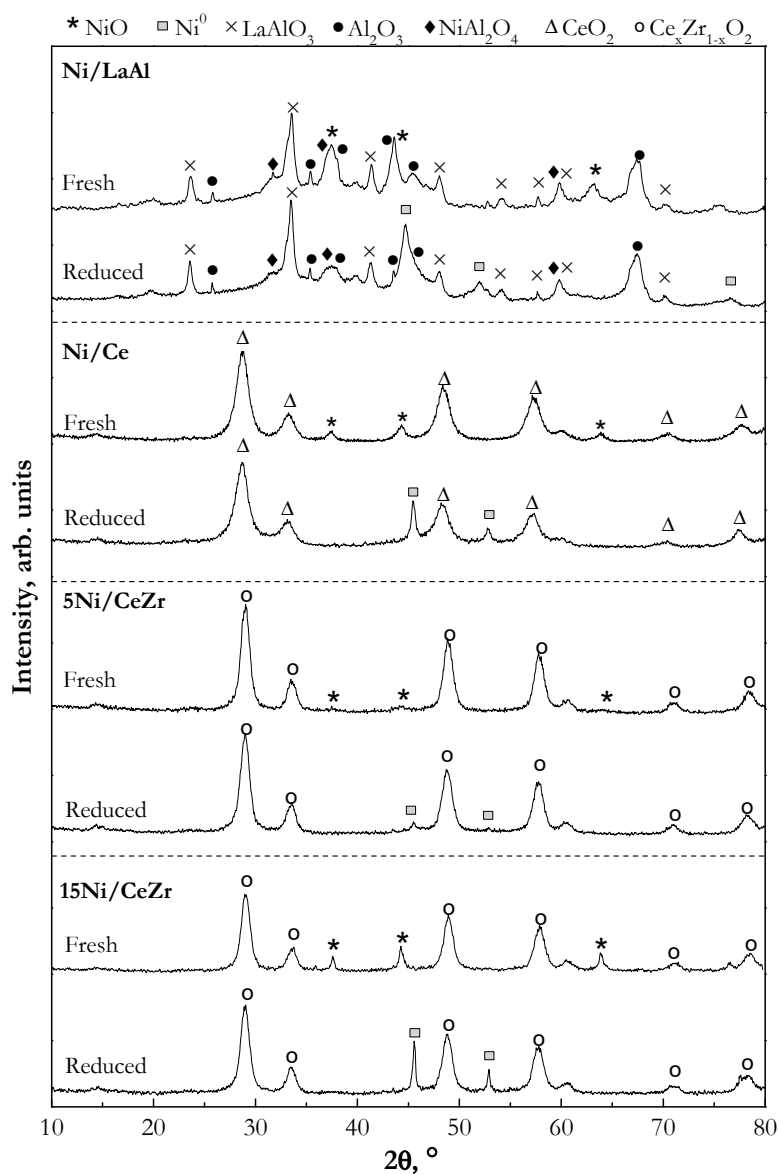

Figure 3. The X-ray diffractograms of the synthetized Ni supported catalysts, prior to reduction (fresh) and after reduction at 700 °C.

The diffraction peaks corresponding to NiO (fresh samples) and Ni^0 (reduced samples) are also observed for the catalysts supported on Ce or CeZr (Ni/Ce, 5Ni/CeZr, and 15Ni/CeZr), although the peaks of these phases for 5Ni/CeZr catalyst are of low intensity due to its low Ni content (5 wt %). Peaks corresponding to CeO$_2$ phase are also identified in the diffractograms of the three catalysts, which are characteristic of the fluorite structure [51,52]. The doping of CeO$_2$ with ZrO$_2$ (5/NiCeZr and 15Ni/CeZr catalysts) slightly shifts the peaks of the CeO$_2$ support towards higher values of diffraction angle (2θ), which is characteristic of the incorporation of Zr^{+4} ions in the structure of CeO$_2$ [53,54].

The X-ray diffractogram of the reduced commercial G90 catalyst was reported elsewhere [55], and it evidenced a complex structure, with up to six crystalline phases corresponding to Ni^0, NiO, Al$_2$O$_3$, CaO(Al$_2$O$_3$)$_2$, CaAl$_2$O$_4$, and CaAl$_{12}$O$_{19}$.
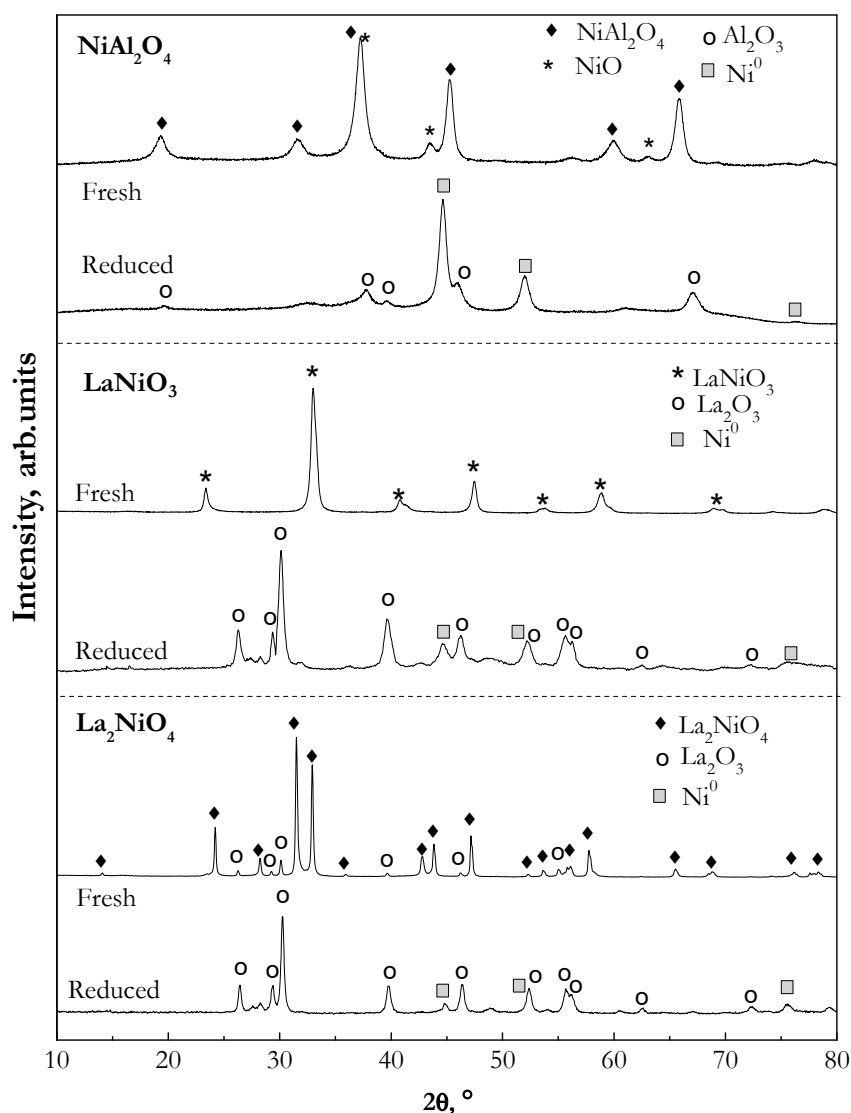

Figure 4. The X-ray diffractograms of the bulk catalysts, type perovskite Ni-La and spinel NiAl$_2$O$_4$, prior to reduction (fresh) or after reduction.

The only phase observed in the X-ray diffractogram of the LaNiO$_3$ perovskite prior to reduction is LaNiO$_3$ (Figure 4), which evidences the efficiency of the auto-combustion method used for obtaining this catalyst. Nevertheless, in the X-ray diffractogram of the La$_2$NiO$_4$ perovskite, the presence of La$_2$O$_3$ species is observed, together with La$_2$NiO$_4$, which could be due to the need of a higher calcination temperature or to a defect in the amount of the fuel (glycine) in the synthesis by auto-combustion,

which hampers the compete combustion reaction [56]. After the reduction of both perovskite-type catalysts, the only species observed are Ni^0 and La_2O_3. The X-ray diffractogram of the fresh $NiAl_2O_4$ catalyst shows diffraction peaks corresponding to two different Ni species, $NiAl_2O_4$ and NiO, in agreement with the TRP profile in Figure 2, whereas in the diffractogram of the reduced sample the only species identified are Ni^0 and Al_2O_3, which proves the complete reduction of Ni^{2+} in the spinel phase to Ni^0.

By means of the Scherrer equation, the average Ni^0 crystallite size has been determined for all the catalysts (Table 3). The value corresponding to the diffraction angle $2\theta = 51.8$ has not been estimated for 5Ni/CeZr catalyst due to the low intensity of the corresponding diffraction peak. This value is not shown for the perovskites either, because the peak corresponding to La_2O_3 phase overlaps and interferes highly with the signal.

The lower Ni^0 particle size corresponds to the Ni/LaAl catalyst, with an average size near 8 nm. The average particle size for the rest of the catalysts is significantly higher, which evidences the stabilizing effect of the LaAl support (mainly the La_2O_3 phase), which attenuates the aggregation of metal particles during the reduction [57,58]. The increase in Ni content from 5 to 15 wt % disfavours its dispersion in the CeZr support, with an increase in the average crystallite size from 21.4 to 34.2 nm. Regarding the bulk catalysts, the perovskites have a crystallite size lower than the $NiAl_2O_4$ spinel, which is coherent with the previously mentioned stabilizing effect of La_2O_3 for attenuating the agglomeration of the metal. The higher crystallite size in the $LaNiO_3$ catalyst (14.2 nm) compared to the La_2NiO_4 catalyst (11.6 nm), has been also previously observed by Guo et al. [42], who attributed this result to the higher content of Ni in the $LaNiO_3$ catalysts, which hinders its dispersion.

Table 3. The average size of the Ni^0 crystallite for the reduced supported and bulk catalysts, determined from diffraction angles 44.5° (plane 111) and 51.8° (plane 200).

Catalyst	dNi^0, nm (44.5°) *Plane (1 1 1)*	dNi^0, nm (51.8°) *Plane (2 0 0)*
Supported catalysts		
Ni/LaAl	8.7	7.6
Ni/Ce	23.4	20.5
5Ni/CeZr	21.4	-
15Ni/CeZr	34.2	30.7
G90* [59]	24.0	-
Bulk Catalysts		
$LaNiO_3$	14.2	-
La_2NiO_4	11.6	-
$NiAl_2O_4$	17.5	13.0

2.2. Performance of the Catalysts

The performance of the catalysts in the OSR of raw bio-oil has been compared under the operating conditions indicated in Section 4.3, which were selected according to the previous results on the SR and OSR of bio-oil [15,21,26,27]. These conditions (700 °C, S/C = 6, O/C = 0.34, with low space-time values) provide high bio-oil conversion and H_2 yield, but with quite a rapid deactivation of the catalysts (due to the low space-time), in order to allow a rapid comparison of the catalysts stability. The results corresponding to the supported catalyst are presented in Section 2.2.1, whereas those corresponding to the bulk catalysts (together with the best-supported catalyst) are compared in Section 2.2.2.

2.2.1. Supported Catalysts

The evolution with time on stream of bio-oil oxygenates conversion (Figure 5a), H_2 yield (Figure 5b) and yields of the carbon products (CO_2, CO, CH_4 and hydrocarbons C_2-C_4, hereafter denoted HCs) (Figure 5c–f) for the supported Ni catalysts is shown in Figure 5. The dashed lines

identify the values obtained by means of thermal routes (without catalyst), and these are the values obtained when the catalyst is completely deactivated.
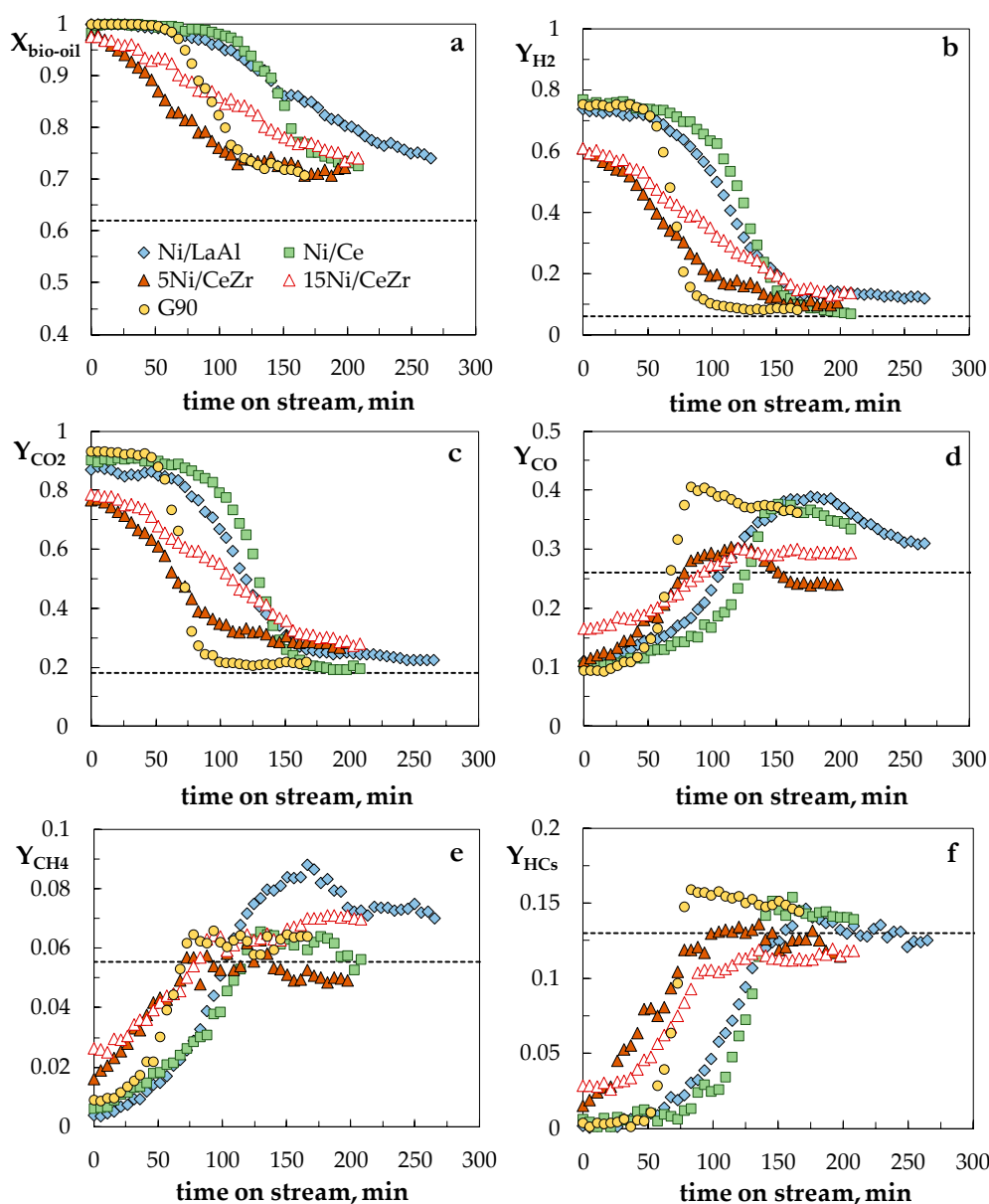

Figure 5. The comparison of the evolution with time on the stream of bio-oil conversion (**a**), yield of H_2 (**b**), and yields of CO_2, CO, CH_4, and HCs (**c**–**f**) with the Ni supported catalysts. Reaction conditions: 700 °C; S/C, 6; O/C, 0.34; space-time, 0.3 $g_{catalyst}h(g_{bio-oil})^{-1}$.

As observed, all the catalysts are highly active for the OSR of raw bio-oil at zero time on stream, with complete or almost complete bio-oil conversion (Figure 5a). Nevertheless, important differences are observed in the products distribution, H_2 selectivity, and the stability for the different catalysts.

Firstly, the difference in the products yield at zero time on stream for the catalysts supported on CeZr with respect to the rest of the Ni supported catalysts is remarkable. Thus, the yields of H_2 (~60%, Figure 5b) and CO_2 (~77%, Figure 5c) are noticeably lower than those obtained with Ni/LaAl, Ni/Ce and G90 catalysts (in the range 74–78% for H_2 and 89–94% for CO_2), whereas the yields of CO, CH_4 and HCs are higher (Figure 5d,e). These differences give evidence that the synthetized Ni/CeZr catalysts are less active for oxygenates reforming reactions and WGS reaction, and also for the reforming of the

by-products (CH_4 and HCs) formed by the decomposition/cracking of oxygenates. Moreover, in the studied conditions, the variation in the Ni content in the catalysts supported on CeO_2-ZrO_2 does not have a relevant effect on the initial products distribution, but it only affects the catalysts deactivation rate. Thus, as expected, the deactivation rate is apparently attenuated when the Ni content is increased due to the higher extent of reaction when the number of active sites is increased (that is, when operating more close to the thermodynamic regime). Consequently, the differences in the products selectivity at zero time on stream observed in Figure 5 should be attributed to the different supports and not to the Ni content, which evidences the support contribution in the reaction mechanism.

Attending to catalysts stability, the similar evolution with time on the stream of the reaction indices in Figure 5 for the Ni/LaAl, Ni/Ce, and G90 catalysts is remarkable. Thus, after an initial stable period (in which the reaction indices are almost constant—as there is an excess of the catalyst in these conditions) there is a rapid deactivation period (breakthrough curves). In this deactivation period, there is a rapid decrease in conversion and yields of H_2 and CO_2, and in parallel a rapid increase in the yields of CO, CH_4 and HCs up to a maximum, which gives evidence that deactivation noticeably affects the oxygenates reforming and WGS reactions, and also the reforming of CH_4 and HCs. Nevertheless, it is interesting to note that, in general, the increase in the yield of HCs with the time on stream slightly delayed with respect to the increase in CH_4 yield, seems to indicate that the CH_4 reforming reaction is more affected by deactivation than the HCs reforming reaction, because the former requires a more active catalyst. Moreover, a last period, with very slow and progressive deactivation, is observed (subsequent to the maximum in the yields of CO, CH_4 and HCs) with the reaction indices slowly approaching the values corresponding to the thermal routes (without a catalyst), which are those depicted with dashed lines. With the commercial G90 catalyst, the initial stable period is shorter and the subsequent variation with the time on stream of the reaction indices is faster than with the synthetized Ni/LaAl and Ni/Ce catalysts, which evidences the more rapid deactivation of the commercial catalyst. The initial stable period is slightly shorter for the Ni/LaAl catalyst than for the Ni/Ce catalyst, which could be attributed to the lower Ni content in the former, although the difference is small. Moreover, it is remarkable that the slope of the breakthrough curve is less abrupt with the Ni/LaAl catalyst, which indicates a slower deactivation rate for this catalyst.

The evolution with the time on stream of the reaction indices for the Ni/CeZr catalysts in Figure 5 is significantly different to that previously commented. Thus, a progressive and slower decrease in bio-oil oxygenates conversion and yields of the main products (H_2 and CO_2) is observed from the beginning of the reaction, and in parallel an increase in the yields of by-products (CO, CH_4 and HCs), with a slower variation in the reaction indices (and, consequently, a slower deactivation) for a higher Ni content.

The residual activity of the catalysts at the end of the runs should be noted so that the bio-oil conversion and the yields of products are significantly different from the values corresponding to the thermal routes (dashed lines, runs without catalyst), which indicates that the catalysts are not completely deactivated. Thus, the high CO yields for the Ni/LaAl, G90 and Ni/Ce catalysts indicate that these catalysts keep a residual activity for oxygenates reforming reactions and a high activity for the oxygenates cracking/decomposition reaction, in which CO is formed, together with H_2, CH_4, and HCs.

Attending to the results in Figure 5, it can be concluded that, among the studied Ni supported catalysts, the best performance in the OSR of raw bio-oil corresponds to Ni/LaAl, as it provides the better compromise between activity-H_2-selectivity-stability.

2.2.2. Bulk Catalysts

The behaviour in the OSR of raw bio-oil of the bulk Ni-La perovskites (the $LaNiO_3$ and La_2NiO_4 catalysts) and the $NiAl_2O_4$ spinel catalyst is shown in Figure 6 (conversion of oxygenates in bio-oil (Figure 6a), H_2 yield (Figure 6b) and yield of the carbon products (Figure 6c–f)). In these graphs, the results for Ni/LaAl catalyst are also shown, as it has the better performance among the supported

catalysts according to the results in the previous section. Attending to the big differences in the metal content for the bulk catalysts, the comparison of their performance has been assessed in experiments with the same value of space-time referred to the metal content in the catalyst (0.03 $g_{Ni}h(g_{bio-oil})^{-1}$).
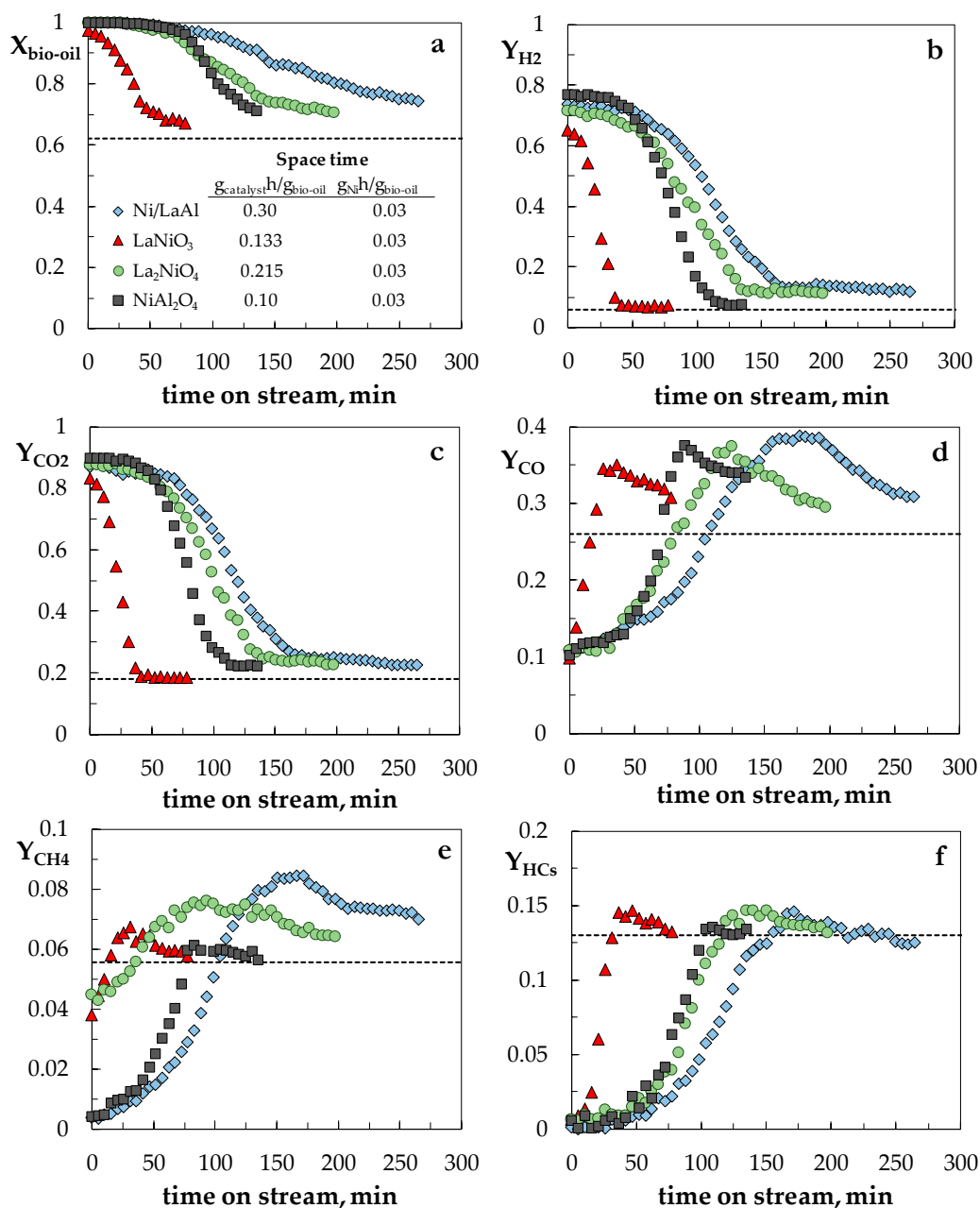

Figure 6. The comparison of the evolution with time on the stream of bio-oil oxygenates conversion (**a**), yield of H_2 (**b**) and yields of CO_2, CO, CH_4, and HCs (**c**–**f**) with the bulk catalysts and the Ni/LaAl catalyst. Reaction conditions: 700 °C; S/C, 6; O/C, 0.34, space-time, 0.03 $g_{Ni}h(g_{bio-oil})^{-1}$.

As observed, the $LaNiO_3$ catalyst is less active than the other three catalysts as it does not reach total bio-oil conversion at zero time on stream (Figure 6a), and it has the lowest H_2 yield. An important difference is also observed in the products distribution at zero time on stream with the two perovskite-type catalysts compared to the supported Ni/LaAl and bulk $NiAl_2O_4$ spinel catalysts. Thus, with the former, the CH_4 yield is noticeable higher (around 0.05, whereas it is almost null for the Ni/LaAl and $NiAl_2O_4$ spinel catalyst), and, consequently, the H_2 yield is lower

(between 0.63–0.71 for the perovskite catalysts, whereas it is 0.74 and 0.77 for Ni/LaAl and NiAl$_2$O$_4$, respectively). This result evidences the lower activity of the Ni-La perovskite catalysts for the CH$_4$ reforming reaction and, moreover, the importance of Al$_2$O$_3$ support for promoting this reaction [59]. Nevertheless, the perovskite catalysts are highly active for the reforming of light hydrocarbons, whose yield at zero time on stream is negligible, similarly to the Ni/LaAl and NiAl$_2$O$_4$ catalysts.

Regarding the bulk catalysts stability, the results in Figure 6 evidence that LaNiO$_3$ perovskite deactivates much more rapidly than the rest of the catalysts. Guo et al. [42] also observed a higher activity and stability of La$_2$NiO$_4$ perovskite over LaNiO$_3$ perovskite in the partial oxidation of methane, which was attributed to the stronger interaction between Ni and La$_2$O$_3$ in the La$_2$NiO$_4$ catalyst and its lower acidity, which caused a lower coke deposition.

To sum up, the results in this section give evidence that the Ni/LaAl catalyst has a better performance in the OSR del raw bio-oil than the bulk catalysts studied, both concerning the conversion and H$_2$ selectivity (especially compared to LaNiO$_3$ perovskite) and the catalyst stability (when compared to the La$_2$NiO$_4$ perovskite and NiAl$_2$O$_4$ spinel catalysts). Among the bulk catalysts, the NiAl$_2$O$_4$ spinel catalyst has a more interesting behaviour for the OSR of bio-oil, because of its higher H$_2$ selectivity compared to the perovskite-type catalysts, although it deactivates slightly faster than the La$_2$NiO$_4$ perovskite.

2.3. Analysis of Coke Deposition (Temperature Programmed Oxidation (TPO))

The coke deposited on the deactivated catalysts has been analysed by temperature programmed oxidation (TPO) analysis. This technique provides information concerning the total coke content and the nature and/or location of the deposited coke (based on the position of the combustion peaks in the TPO profile), which is of interest for relating it with the deactivation rate and with the properties of the catalysts. It is well established that the deposition of coke is the main deactivation cause in the reforming of pure oxygenates and of bio-oil [60]. Moreover, the TPO profile provides information on the minimum temperature required for assuring total coke removal, which will be necessary in order to recover the activity of the fresh catalyst. Figure 7 shows the TPO profiles for some of the deactivated catalysts, specifically for Ni/LaAl and Ni/Ce (those with the better performance among the supported catalysts) and for the NiAl$_2$O$_4$ spinel.
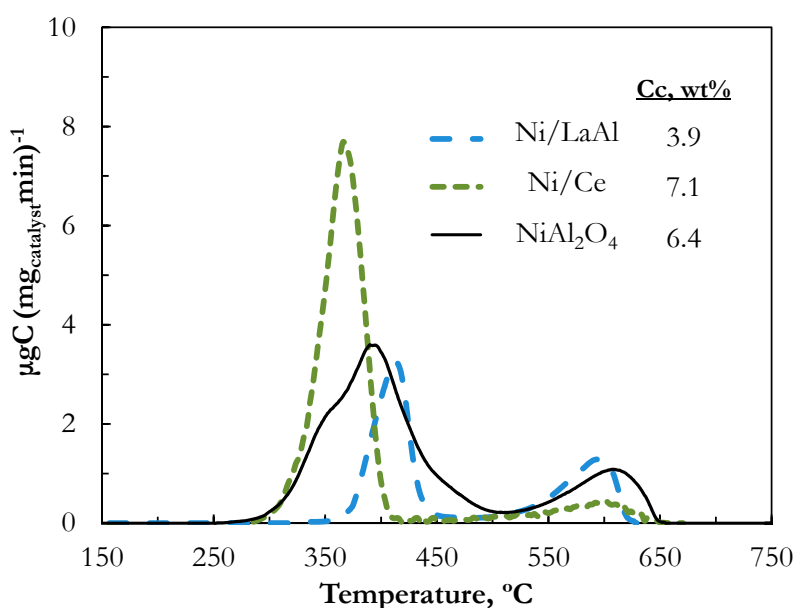

Figure 7. The TPO profiles for supported Ni/Ce and Ni/LaAl and bulk NiAl$_2$O$_4$ spinel catalyst.

For all the catalysts, two different combustion domains are observed: the main peak burns at low temperature, in the 300–450 °C range, and the position of its maximum differs depending on the nature of the support, in the order Ni/Ce < $NiAl_2O_4$ < Ni/LaAl; the minority peak burns at high temperature, with a maximum near 600 °C. In the literature, the first peak is attributed to the combustion of encapsulating coke of amorphous nature and deposited on the metal sites (that catalyse the combustion reaction at a lower temperature), thus having a high impact on deactivation. The coke burning at high temperature is attributed to a more structured coke (with a high content of condensed polyaromatics) deposited on the support and, consequently, with a lower impact on deactivation [26,27,61]. The low content of coke deposited on the support for Ni/Ce catalyst could be explained by the redox properties of the CeO_2 support and its capacity for O_2 storage, which enhances the lattice oxygen exchange with O_2 in the gas phase and favours coke gasification during the reaction [62]. This property of CeO_2 could have a synergistic effect for promoting the combustion of encapsulating coke towards a lower combustion temperature.

From the results in Figure 7, it is concluded that 650 °C is the temperature at which occurs the complete removal—by combustion with air—of the coke deposited in the deactivated catalysts.

2.4. Regenerability of the Catalyst

The recovery of activity after the coke combustion has been determined by comparing the evolution with the time on stream of the reaction indices obtained with the regenerated catalyst to those of the fresh catalyst, with runs under reaction-regeneration cycles. The regeneration has consisted of coke combustion with air at a temperature that assures the total removal of coke, as it is assumed to be the main cause of deactivation in reforming processes. Firstly, the combustion was carried out in the fluidized bed reactor at 650 °C, as this is the minimum temperature necessary according to the results in Figure 7. The comparison of the reaction indices (bio-oil conversion and yields of H_2 and CO_2) for the fresh catalyst (1st reaction) and the regenerated catalyst (2nd reaction) for the supported and the bulk catalysts is shown in Figures S1 and S2, respectively, of the Supplementary Material. These figures evidence that, although coke is completely removed, none of the studied Ni catalyst recovers the initial activity corresponding to the fresh catalyst after coke combustion with air in the fluidized bed reactor at 650 °C. Thus, the initial values of bio-oil conversion and H_2 yield for the regenerated catalysts are only slightly higher to those obtained at the end of the first reaction, and similar to those obtained for an intermediate time on stream value in the first reaction. Other authors have also previously reported the difficulty for activity recovery after different regeneration strategies for Ni-based catalysts used in the reforming of oxygenates [63–65].

The aforementioned results evidence that a regeneration treatment consisting of coke combustion at 650 °C is not efficient for the recovery of the activity of the studied Ni catalysts, which could be due to several causes. On the one hand, the existence of an additional deactivation cause, besides coke deposition, such as Ni sintering due to the high temperature and water content in the reaction medium [61,66]; on the other hand, there could be metal loss due to the detachment during coke combustion of some Ni^0 particles located at the edges of the coke filaments. Consequently, the regeneration treatment should be able not only to remove coke but also to re-disperse the Ni particles, and moreover, the loss of Ni during the regeneration should be avoided.

Recently, Remiro et al. [66] have reported that a bulk $NiAl_2O_4$ spinel catalyst prepared by co-precipitation completely recovered the activity of the fresh catalyst after a regeneration treatment consisting of coke combustion in an air atmosphere at 850 °C in an external oven. The activity recovery was attributed to the total recovery of the spinel structure of the fresh catalyst under these severe regeneration conditions, which favoured the reconstruction of the $NiAl_2O_4$ spinel by reaction of NiO with Al_2O_3 in the support. Subsequently, the reduction step of the spinel produced well-dispersed Ni^0 particles, whereas the reduction of the prevailing NiO species formed by a coke combustion at 650 °C produced Ni^0 particles of a higher size, and consequently, of lower activity. Based on these previous results, in this work, we have analysed the activity recovery of the bulk catalysts (perovskite

La$_2$NiO$_4$ and spinel NiAl$_2$O$_4$, prepared by auto-combustion in this study) subsequent to a regeneration treatment by coke combustion in an external oven at high temperature (850 °C), and the results are depicted in Figures 8 and 9. In these figures, the evolution with the time on stream of bio-oil conversion and H$_2$ yield in the first reaction step (fresh catalysts) and subsequent reaction steps (regenerated), is plotted for spinel NiAl$_2$O$_4$ (Figure 8) and perovskite La$_2$NiO$_4$ (Figure 9).
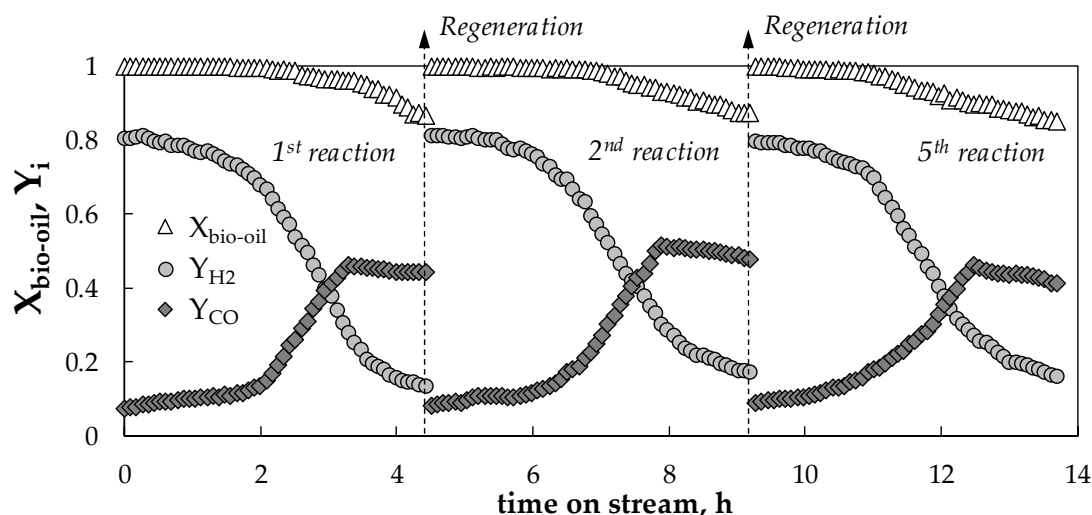

Figure 8. The evolution with the time on stream of bio-oil conversion and yields of H$_2$ and CO in the OSR de bio-oil with the spinel NiAl$_2$O$_4$ catalysts fresh (1st reaction) and regenerated (2nd and 5th reactions). Reaction conditions: 700 °C, space-time, 0.15 g$_{catalyst}$h(g$_{bio-oil}$)$^{-1}$, O/S/C = 0.34/6/1. Regeneration: at 850 °C in an external oven.
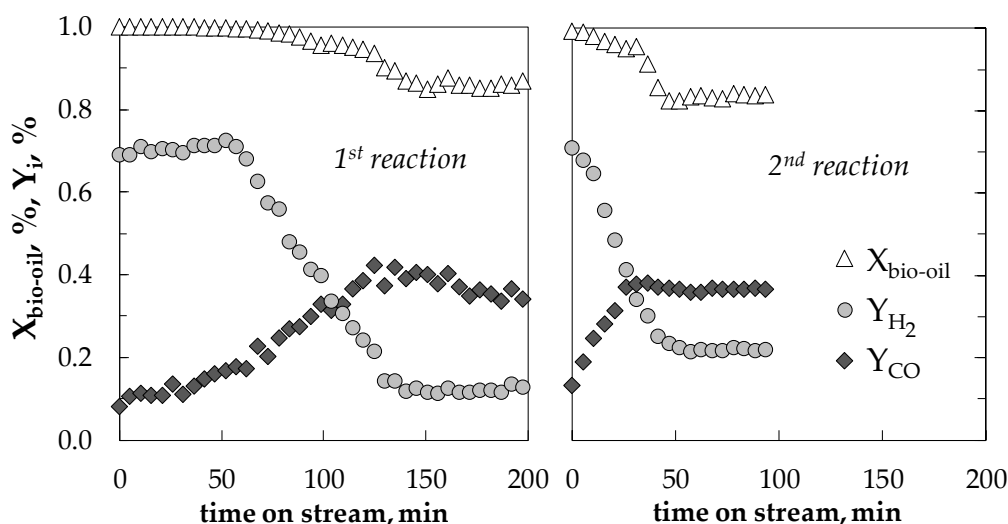

Figure 9. The evolution with the time on stream of bio-oil conversion and yields of H$_2$ and CO in the OSR de bio-oil with the La$_2$NiO$_4$ perovskite catalyst, fresh (1st reaction) and regenerated (2nd reaction). Reaction conditions: 700 °C, space-time, 0.22 g$_{catalyst}$h(g$_{bio-oil}$)$^{-1}$, O/S/C = 0.34/6/1. Regeneration: coke combustion at 850 °C in an external oven.

The results in Figure 8 are in agreement with the results previously obtained by Remiro et al. [66] for the bulk spinel catalyst prepared by the co-precipitation method, and consequently, it can be deduced that the total activity recovery subsequent to the regeneration by coke combustion at 850 °C

in the external oven (in an air atmosphere, without gas flow) is a general property of the bulk $NiAl_2O_4$ spinel catalysts, regardless of the method for synthetizing the fresh catalyst.

On the contrary, the comparison of the reaction indices in the first and second reaction step for the La_2NiO_4 perovskite (Figure 9) shows that the activity recovered after the regeneration at 850 °C in an external oven is much higher than that recovered by regeneration at 650 °C in the fluidized bed reactor (Figure S2a), but it is not complete. This difficulty for restoring the metal species present in the fresh La_2NiO_4 catalyst after the regeneration by coke combustion with air has been proved by comparing the XRD profile of the fresh catalyst and the regenerated catalysts (Figure 10). As observed in Figure 10, there are differences between the fresh and the regenerated catalysts; in the latter, the presence of $LaNiO_3$ is observed (whose lower activity compared to La_2NiO_4 has been proven in Section 2.2.2), which involves a lower activity for the regenerated catalyst. The XRD diffractogram of the catalyst regenerated at 850 °C in an external oven is more similar to that of the fresh catalyst than that of the catalyst regenerated in the fluidized bed at 650 °C, although the presence of $LaNiO_3$ is also observed. These differences in the metal species are responsible for the different activity recovered after each regeneration treatment.
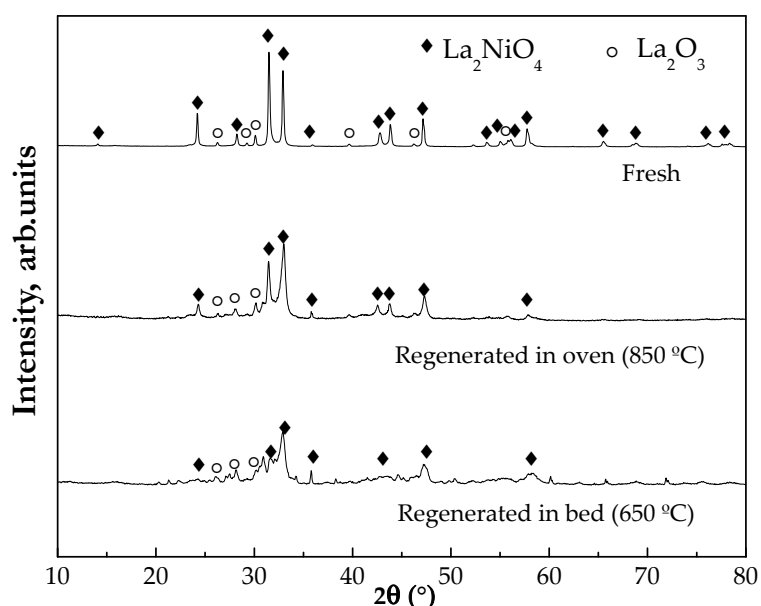

Figure 10. The XRD diffractograms for La_2NiO_4 catalyst fresh and regenerated in different conditions.

It should be mentioned that the regeneration results at a high temperature have not been studied for the supported catalysts, as all of them were synthetized with a low calcination temperature (550 °C), and consequently, the combustion at a significantly higher temperature is expected to negatively affect the metallic structure of these catalysts.

3. Discussion

Attending to the results in Figure 5, and considering the target of a better compromise between activity, H_2 selectivity and stability, the following order of interest in the OSR of raw bio-oil can be established for the supported Ni catalysts:

$$Ni/LaAl > Ni/Ce \gg G90 > 15Ni/CeZr > 5Ni/CeZr$$
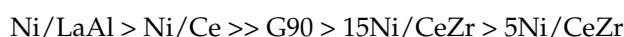
This order can be related with the Ni^0 crystallite size in the catalysts, calculated from XRD diffractograms (Table 3), and proves the relevance of this property of Ni catalyst in its activity and stability. Thus, the better performance corresponds to the Ni/LaAl catalyst, which has the lower

average Ni particle size ($\approx$8 nm) and, consequently a high specific metal surface, which is more important than the Ni content, which is lower (10 wt %) than in the Ni/Ce catalyst (15 wt %), and justifies that both have a similar initial activity in the bio-oil reforming. Moreover, the relationship between the rate of coke deposition (the main deactivation cause of Ni catalysts) and the Ni^0 crystallites size is well established in the literature [67–69]. The better performance of the Ni catalysts supported on Al_2O_3 with respect to those supported on CeO_2-ZrO_2 has been observed by other authors in the reforming of oxygenates [70,71] and CH_4 [72]. It is assumed that the interaction of NiO with CeO_2-ZrO_2 support is weaker, which makes metal reduction easier, but also favours the agglomeration of the Ni crystallites in the reducing atmosphere. The lower Ni particles size in the Ni/LaAl catalyst than in Ni/Ce, in spite of the noticeably higher specific surface area of the Ce support compared to the LaAl support, gives evidence that, when preparing the catalysts by impregnation, the metal-support interaction (higher in Ni/LaAl catalyst) has a higher impact on the crystallites size than the specific surface area of the support. A higher size of Ni^0 crystallites involves a lower initial activity and a lower stability due to the more rapid coke deposition and also more rapid sintering of the Ni crystallites during the reaction.

The results in Figure 6, also prove the better performance in the OSR of bio-oil of the Ni/LaAl catalyst compared to the bulk catalysts, with a stability of the catalysts in the order:

$$Ni/LaAl > La_2NiO_4 > NiAl_2O_4 >> LaNiO_3$$
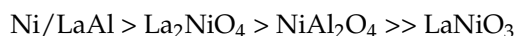
This order is also related to the average particle size of the Ni^0 crystallites (Table 3), which has a relevant role in the activity and stability of the catalysts, as commented for the supported catalysts. Thus, the better performance of La_2NiO_4 over $LaNiO_3$ is coherent with the lower average size of Ni^0 crystallites (11.6 and 14.2 nm, for the reduced La_2NiO_4 and $LaNiO_3$ catalysts, respectively). Similarly, the higher stability of Ni/LaAl over the $NiAl_2O_4$ spinel (both with a similar support) is coherent with the noticeable lower particle size for the former. Moreover, the effect of the support seems to be also relevant in the catalytic activity, so that a higher H_2 selectivity is obtained for the catalysts with Al_2O_3 in the support over the Ni-La perovskites, because the former favours the methane reforming reaction.

As shown in Figures 5 and 6, the deactivation of the catalysts in the OSR of raw bio-oil is unavoidable. Although it can be attenuated with operating conditions suitable for minimizing its possible causes (such as high space-time values and S/C ratios for minimizing coke deposition [27]), the industrial development of the process will require using regeneration strategies that allow the complete recovery of the activity corresponding to the fresh catalyst. Consequently, together with a high activity, H_2 selectivity, and stability in the reaction, the regenerability of the catalyst (that is, the ability for recovering the activity of the fresh catalysts subsequent to a suitable regeneration strategy), is a key factor for the selection of the catalyst. The results in Section 2.3 prove that the total removal of coke is not enough for the recovery of the activity of the Ni catalysts used in the OSR of raw bio-oil, which should be attributed to the existence of other deactivation causes besides coke deposition, such as metal sintering or changes in the metal species. The sintering of Ni at 700 °C has been previously reported for Ni/LaAl catalyst used in the SR of bio-oil [15,61] for the commercial G90 catalysts used in the SR of biomass pyrolysis volatiles [73] and for spinel $NiAl_2O_4$ catalysts prepared by different methods and used in the OSR of bio-oil [66]. Besides the changes in the metallic structure originated in the reaction step, the effect of the operating conditions in the regeneration step upon the physical-chemical properties of the catalyst (especially the metal properties) should be also considered, as they would be responsible for the activity of the regenerated catalyst.

Remiro et al. [66] have proven the relevance of the operating conditions in the regeneration step by coke combustion on the metallic properties of two $NiAl_2O_4$ spinel type catalysts (one of them obtained by calcination at 850 °C of a Ni/La_2O_3-Al_2O_3 supported catalyst and the other was a bulk catalyst prepared by co-precipitation and also calcined at 850 °C) used in the OSR of raw bio-oil. It was proven that the temperature and the gas-solid contact in the regeneration by coke combustion have a significant effect in the formation of different oxidized Ni species (NiO and $NiAl_2O_4$), which is a

key factor for the redispersion of the Ni^0 active sites after the reduction and, consequently, for the recovery of the catalyst's activity. For both catalysts, coke combustion at high temperature (850 °C) in an external oven (air atmosphere, without catalyst motion or gas flux) promoted the creation of "hot spots" and enhanced the contact between NiO and Al$_2$O$_3$, which favoured their reassembly to form a NiAl$_2$O$_4$ spinel phase in the regenerated catalyst, which after reduction resulted in small and well dispersed Ni^0 particles. On the contrary, when the regeneration was carried out by coke combustion with air in the fluidized bed reactor at lower temperatures, the prevailing Ni species in the regenerated catalyst was NiO, which after reduction formed large metal particles (of lower activity). Under these optimum regeneration conditions, the activity recovery of the bulk NiAl$_2$O$_4$ spinel catalyst prepared by co-precipitation was complete, but partial for the supported catalyst, which proved the relevance of the structure of the fresh catalyst in its regenerability. This different activity recovery of both catalysts (supported and bulk) was explained by their different capability to retain the Ni surface species throughout a reaction-regeneration cycle so that the loss of Ni (mainly on the surface) was high for the supported catalyst.

In this work, the total recovery of activity subsequent to a regeneration treatment at high temperature (850 °C in an air atmosphere, but without gas flux) has been proved for a bulk spinel catalyst prepared by auto-combustion. This result evidences that the high activity recovery is a general characteristic of bulk spinel type catalysts, regardless of the procedure for synthetizing the bulk NiAl$_2$O$_4$ spinel. Nevertheless, the bulk perovskite La$_2$NiO$_4$ catalyst does not completely recover the activity corresponding to the fresh catalyst after regeneration by coke combustion at 850 °C, which should be attributed to the difficulty for completely restoring the initial metallic structure of the fresh catalyst. Similarly, the total recovery of activity for the supported catalysts is expected to be hampered by the difficulty in restoring the corresponding metallic structure of the corresponding fresh catalyst subsequent to the coke removal by combustion with air at a temperature higher than those used in the calcination and reduction of the catalysts.

From all these comments concerning the regenerability of the Ni-based catalysts, it can be concluded that the spinel NiAl$_2$O$_4$ catalyst is the more suitable option for developing the reforming of bio-oil at an industrial level. This catalyst has a slightly lower activity and stability compared to the supported Ni/LaAl catalyst, but it allows a reproducible performance in successive reaction-regeneration cycles. On the contrary, the Ni/LaAl catalyst suffers from irreversible deactivation due to the difficulty for redispersing Ni particles subsequent to coke combustion, although the activity loss is expected to attenuate in successive reaction-regeneration cycles, thus tending towards a stationary state [63].

4. Materials and Methods

4.1. Bio-Oil Production and Properties

The raw bio-oil was obtained by flash pyrolysis of pine sawdust at 480 °C, in a semi-industrial demonstration plant (Ikerlan-IK4 technology centre, Alava, Spain), with a biomass feeding capacity of 25 kg/h. The physical-chemical properties of the bio-oil are as follows: water content, 38 wt %; density at 25 °C, 1.107 g mL^{-1}; viscosity at 40 °C, 11.2 cP; pH, 3.3; sulphur content, 31 ppm; empiric formula obtained by CHO analysis, C$_{4.21}$H$_{7.14}$O$_{2.65}$ (dry basis). The detailed raw bio-oil composition, determined by GC/MS analyser (Shimadzu QP2010S device, Kyoto, Japan) was previously reported [15], with the main compounds being acids (33.83 wt %, with 25.25 wt % of acetic acid), ketones (22.63 wt %, with 15.53 wt % of 1-hidroxi-2-propanone), aldehydes (8.19 wt %, with 4.53 wt % hydroxiacetaldehyde), phenols (11.57 wt %), and sacarids (16.90 wt %, with 14.61 wt % levoglucosane).

4.2. Synthesis and Characterization of the Catalysts

Table 4 gathers the simplified denomination of the synthesized catalysts, which have been grouped into supported (upon metal oxides, La_2O_3-αAl_2O_3, CeO_2, and CeO_2-ZrO_2) and bulk catalysts (with a Ni-Al spinel structure and Ni-La perovskite structure). The nominal metal content and the calcination and reduction temperatures (T_C and T_R, respectively) are also shown in Table 4.

Table 4. The composition, nominal metal content, calcination temperature, and preparation method of the synthesized catalysts.

	Catalyst	Name	Nominal Ni Content, wt %	T_C, °C	T_R, °C
Supported	Ni/La_2O_3-αAl_2O_3	Ni/LaAl	10% Ni	550	700
	Ni/CeO_2	Ni/Ce	15% Ni	550	700
	Ni/CeO_2-ZrO_2	5Ni/CeZr	5% Ni	550	700
		15Ni/CeZr	15% Ni		
Bulk	$NiAl_2O_4$ spinel	$NiAl_2O_4$	33% Ni	850	850
	$LaNiO_3$ perovskite	$LaNiO_3$	23.9% Ni	700	700
	La_2NiO_4 perovskite	La_2NiO_4	14.6% Ni		

The supported catalysts have been prepared by incipient wetness impregnation of the corresponding support by using a solution of $Ni(NO_3)_2 \cdot 6H_2O$ (99%, Panreac, Barcelona, Spain,) for Ni impregnation.

The La_2O_3-αAl_2O_3 support (denoted LaAl) was prepared from α-Al_2O_3 (Derivados del Flúor, Bilbao, Spain) (with a particle size between 125–250 µm, and dried at 110 °C for 24 h for removal of surface moisture), which was impregnated with an aqueous solution of $La(NO_3)_3 \cdot 6H_2O$ (99.9%, Alfa Aesar, Haverhill, MA, USA>) (with suitable concentration for obtaining a nominal 10 wt % La in the support) in a rotary evaporator *Buchi R-114* (New Castle, DE, USA), at 65 °C under vacuum. The resulting solid was dried at 110 °C for 24 h and was calcined at 900 °C for 3 h [74].

The CeO_2 support (Ce) was synthesized from an aqueous solution of $Ce(NH_4)_2(NO_3)_6$ (99.9%, Sigma-Aldrich, St. Louis, MO, USA) which was added dropwise to a NH_4OH solution under continuous stirring until complete precipitation, at a pH near 9.5. The obtained material was heated up to 100 °C for 96 h, it was then centrifuged and washed with deionized water until the filtered water reaches a pH of 7. Finally, it was dried at 120 °C for 12 h and calcined at 500 °C for 12 h.

The CeO_2-ZrO_2 support (CeZr), with mass ratio 80/20, was prepared from an aqueous solution with the corresponding stoichiometric amounts of $Ce(NH_4)_2(NO_3)_6$ and $ZrO(NO_3)_2$ (35%, Sigma-Aldrich, St. Louis, MO, USA), to which a KOH solution (20 wt %) was added dropwise, under constant pH (10.5) and temperature (80 °C). The precipitate is maintained at 80 °C for 72 h, washed with distilled water and dried in two steps, firstly at room temperature for 48 h and then at 120 °C for 6 h. Finally, the material is calcined at 800 °C for 6 h [75].

The impregnation of each support with the $Ni(NO_3)_2 \cdot 6H_2O$ solution was also carried out in the *Buchi R-114* rotary evaporator at 65 °C, by using suitable amounts of solution for obtaining the metal nominal content in each catalyst. The obtained solid was dried at room temperature for 24 h and subsequently, it was calcined during 2–4 h at the desired temperature (Table 4). Finally, the catalyst was sieved to the desired particle size (125–250 µm).

The bulk $NiAl_2O_4$ spinel catalyst (with 33 wt % Ni) was prepared by auto-combustion from aqueous solutions of $Ni(NO_3)_2 \cdot 6H_2O$ (99%, Panreac, Barcelona, Spain) and $Al(NO_3)_3 \cdot 9H_2O$ (98%, Panreac, Barcelona, Spain), and with urea (CH_4N_2O, 99.5%, Sigma-Aldrich, St. Louis, MO, USA) as fuel. A stoichiometric ratio of fuel/metal nitrates was used for avoiding residual non-reacted fuel and/or nitrates. The procedure is as follows: the corresponding amounts of Ni and Al nitrates are dissolved with the minimum amount of distilled water, together with the suitable amount of urea, and the mixture is heated in a heating jacket at 80 °C under continuous stirring, thus forming a dark green gel. At that moment, the stirring is stopped, and the heating jacket power is set to its maximum

so that the auto-combustion of the mixture takes place for 1–2 minutes until the fuel is completely consumed. The resulting fine powder is calcined at 850 °C for 4 h (with a heating ramp of 10 °C min^{-1}) thus forming the NiAl$_2$O$_4$ spinel.

The Ni-La perovskite-type catalysts (LaNiO$_3$ and La$_2$NiO$_4$) have been synthesized with the same auto-combustion procedure described for the synthesis of the Ni-Al spinel. The Ni(NO$_3$)$_2$·6H$_2$O and La(NO$_3$)$_3$·6H$_2$O solutions have been used for the synthesis, with suitable proportions for obtaining the required stoichiometry of each catalyst. Both catalysts have been calcined at 700 °C.

All the bulk catalysts were synthetized as powders. For their use in the reforming reactor (in fluidized bed regime), the powdered catalysts were pelletized, ground and sieved for obtaining a particle size between 150–250 µm.

The commercial Ni catalyst (ReforMax® 330 or G90LDP (Sud Chemie, Madrid, Spain), denoted as G90), has a Ni metal phase supported on Al$_2$O$_3$, which is doped with Ca, with a NiO content of 14 wt %. It was provided as perforated rings (19 x 16 mm), which were ground and sieved to 125–250 µm.

The fresh catalysts have been characterized with the following techniques: N$_2$ adsorption-desorption in an *Autosorb iQ2* equipment from *Quantachrome* (Boynton Beach, FL, USA) for determining the physical properties (BET surface area, pore volume, and mean pore diameter); Temperature Programmed Reduction (TPR) on an *AutoChem II 2920 Micromeritics* (Norcross, GA, USA) (H$_2$-N$_2$ stream (10 vol % of H$_2$), with a 5 °C min^{-1} heating ramp from 50 to 900 °C) in order to determine the nature of the Ni species present in the catalyst and the temperature necessary for their total reduction; X-ray diffraction (XRD) on a *Bruker D8 Advance* (Billerica, MA, USA) diffractometer with a CuK$_{\alpha 1}$ radiation, for determining the metal species in the catalysts prior and after reduction, and also for estimating the average Ni particle size (by using the Scherrer equation).

Temperature Programmed Oxidation (TPO) was used for determining the amount and nature of the coke deposited on the deactivated samples. The analysis was carried out in a *TA Instrument SDT 2960* thermobalance (New Castle, DE, USA) (in an air flow of 50 mL min^{-1}, with a heating ramp of 5 °C min^{-1} between 150–800 °C), coupled to a mass spectrometer *Thermostar Balzers Instrument* from *Pfeiffer Vacuum* (Asslar, Germany) for monitoring the signal corresponding to the CO$_2$. The TPO profile was quantified by the CO$_2$ spectroscopic signal because the Ni oxidation during the combustion masks the thermogravimetric signal [66].

4.3. Reaction Equipment, Experimental Conditions, and Reaction Indices

An automated reaction machine (*MicroActivity Reference* from *PID Eng&Tech*, Madrid, Spain) with two units in series (thermal step and catalytic step) was used for the experimental runs which was described elsewhere [15]. Figure 11 shows the scheme of this equipment. The thermal step is a U-shaped tube of stainless steel (at 500 °C) for the controlled deposition of pyrolytic lignin formed by repolymerization of some oxygenates in bio-oil (mainly phenols). In this step, around 11 wt % of the raw bio-oil oxygenate content was deposited as pyrolytic lignin, and the molecular formula corresponding to the bio-oil exiting this step is C$_{3.8}$H$_{7.7}$O$_{2.9}$ (water-free basis), which was determined by elemental balances to C, H, and O. The catalytic step is a fluidized bed reactor (of stainless steel with 22 mm internal diameter) where the volatile stream exiting the thermal treatment is reformed. In order to assure a correct fluidization regime in the fluidized bed reactor, the catalyst (with a particle size of 150–250 µm to avoid internal diffusional limitations) is mixed with an inert solid (SiC, with a 37 µm particle size), with inert/catalyst mass ratio >8/1. The different particle size of the inert solid and the catalysts facilitates their separation after the reaction by sieving, which is necessary for the analysis of coke deposition in the deactivated catalyst.
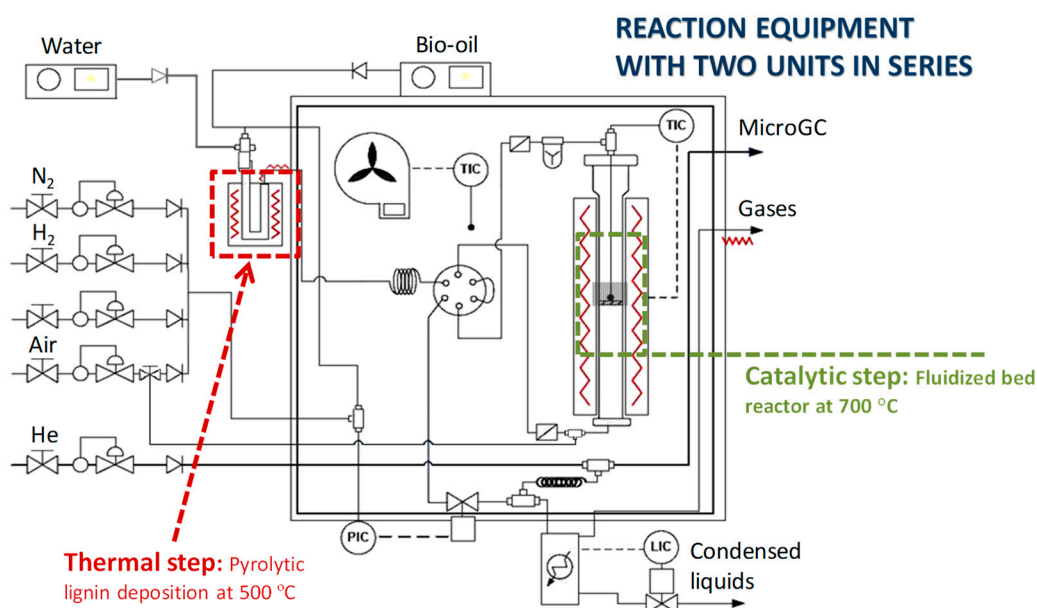
Figure 11. The scheme of the reaction equipment.

The products stream is analysed in-line with a *MicroGC 490* from *Agilent* (Santa Clara, CA, USA), equipped with four analytic channels: a molecular sieve MS5 for quantifying H_2, N_2, O_2, CH_4, and CO; Plot Q for CO_2, H_2O and C_2-C_4 hydrocarbons; CPSIL for C_5-C_{11} hydrocarbons (not detected in this study), and; Stabilwax for oxygenated compounds.

The experimental runs were performed under the following reaction conditions: 700 °C; atmospheric pressure; steam/carbon (S/C) molar ratio in the feed, 6, which is obtained by co-feeding water (*307 Gilson pump*, Middleton, WI, USA) with the raw bio-oil (*injection pump Harvard Apparatus 22*, Holliston, MA, USA); oxygen/carbon ratio (O/C), 0.34. The O_2 is fed at the entrance of the reforming reactor (by means of an air stream) in order to prevent the oxidation of the feed in the thermal step, thus maximizing the H_2 yield in the two-step reaction system [76]. A space-time of 0.3 $g_{catalysts}h(g_{bio-oil})^{-1}$ was used in the runs with the supported Ni catalysts. With the bulk catalysts, attending to their different metal content (defined by its chemical structure, being 14.6 wt % for La_2NiO_4, 23.9 wt % for $LaNiO_3$ and 33 wt % for $NiAl_2O_4$), the comparison of their performance was assessed in experiments with the same value of space-time referred to the metal content in the catalyst (0.03 $g_{Ni}h(g_{bio-oil})^{-1}$). Prior to the reaction, each catalyst is reduced in situ with H_2-N_2 stream (10 vol % of H_2) for 4 h at a suitable temperature for the reduction of all the Ni species in the catalysts, which was determined through TPR measurements (Table 4).

The reaction indices used for the comparison of the kinetic performance of the catalysts include the oxygenates bio-oil conversion, the H_2 yield, and the yield of carbon-containing products, defined by Equations (5)–(7):

$$X_{bio\text{-}oil} = \frac{F_{in} - F_{out}}{F_{in}} \tag{5}$$

$$Y_{H_2} = \frac{F_{H_2}}{F_{H_2}^o} 100 \tag{6}$$

$$Y_i = \frac{F_i}{F_{in}} 100 \tag{7}$$

where F_{in} and F_{out} are the molar flow rate of oxygenates in bio-oil at the reactor inlet and outlet, respectively, in C units contained; F_{H_2} is the H_2 molar flow rate in the product stream and $F^0_{H_2}$ is the stoichiometric molar flow rate (referred to the C units contained in the bio-oil fed into the

reforming reactor); F_i is the molar flow rate of each carbon-containing compound (CO_2, CO, CH_4, and C_2-C_4 hydrocarbons, mainly constituted by ethylene and propylene) in C units contained. The H_2 stoichiometric molar flow rate was calculated as $(2n + m/2 - k)/n \cdot F_{in}$, according to the global stoichiometry for bio-oil steam reforming (SR) (including the water gas shift (WGS) reaction) (Equation (3)).

The flow rates in Equations (5)–(7) have been determined from the C balances with the inlet stream being the bio-oil at the thermal unit inlet (0.08 mL min^{-1}) and the outlet stream the reaction products (quantified by gas chromatography) and taking into account the amount of pyrolytic lignin deposited in the thermal unit. Accordingly, a balance closure above 95 wt % is attained, with the relative error (based on replicates) being lower than 4%.

5. Conclusions

The H_2 production by OSR of raw bio-oil with a wide variety of Ni-based catalysts has been studied by using an experimental equipment with a fluidized bed reactor and with the prior separation of pyrolytic lignin during bio-oil vaporization, thus minimizing operational problems when continuously feeding raw bio-oil. The structure of the catalysts (supported or bulk) and, in the first case, the support composition, significantly affects the deactivation of Ni catalysts by coke deposition and their regenerability. The latter has been studied by means of reaction-regeneration cycles.

Among the Ni supported catalysts (prepared with different Ni contents and supports, and the commercial catalyst G90), the best compromise between activity-H_2 selectivity-stability under OSR conditions follows the order Ni/LaAl > Ni/Ce >> G90 > 15Ni/CeZr > 5Ni/CeZr. This order is directly related to the size of the Ni^0 crystallites of the catalysts, which in turn is highly dependent on the metal-support interaction. Due to the smaller size of the Ni^0 crystallites, the supported Ni/LaAl catalyst also has a better performance than the perovskite-type catalysts $LaNiO_3$ and La_2NiO_4 and that spinel $NiAl_2O_4$.

The TPO analysis for the catalysts reveals two different types of coke: (i) a combustion peak that burns at low temperature, which is an amorphous and encapsulating coke that blocks the Ni active sites, thus causing a rapid deactivation, and; (ii) a peak at high temperature, which is a structured coke, deposited on the support and with lower impact on deactivation. The encapsulating coke is the majority fraction, whose content decreases in the order Ni/Ce > Ni/LaAl (which is opposite to the stability order), and whose combustion temperature depends on the nature of the support, in the order Ce < LaAl, influenced by the good redox properties of CeO_2, that promotes the combustion/gasification of this type of coke. These properties also hinder the formation of structured coke, whose content is only noticeable for the Ni/LaAl catalyst.

The coke combustion with air in the 600–650 °C range allows for the total removal of coke but it is not efficient for the recovery of activity for the Ni catalysts used, which evidences additional deactivation causes, such as Ni sintering, and/or the loss of active metal during the regeneration treatment. The regeneration in an external oven at 850 °C of the $NiAl_2O_3$ spinel prepared by auto-combustion favours the reconstruction of the spinel and the redispersion of Ni in the subsequent reduction step, avoiding the loss of Ni in the regeneration. Consequently, this $NiAl_2O_3$ spinel catalyst is suitable for performing the OSR of bio-oil to a larger scale in reaction-regeneration cycles.

References

1. Sgobbi, A.; Nijs, W.; De Miglio, R.; Chiodi, A.; Gargiulo, M.; Thiel, C. How far away is hydrogen? Its role in the medium and long-term decarbonisation of the European energy system. *Int. J. Hydrogen Energy* **2016**, *41*, 19–35. [CrossRef]

2. Hanley, E.S.; Deane, J.P.; Ó Gallachóir, B.P. The role of hydrogen in low carbon energy futures—A review of existing perspectives. *Renew. Sustain. Energy Rev.* **2017**, *82*, 3027–3045. [CrossRef]

3. Politano, A.; Cattelan, M.; Boukhvalov, D.W.; Campi, D.; Cupolillo, A.; Agnoli, S.; Apostol, N.G.; Lacovig, P.; Lizzit, S.; Farías, D.; et al. Unveiling the Mechanisms Leading to H_2 Production Promoted by Water Decomposition on Epitaxial Graphene at Room Temperature. *ACS Nano* **2016**, *10*, 4543–4549. [CrossRef] [PubMed]

4. Chen, D.; He, L. Towards an efficient hydrogen production from biomass: A review of processes and materials. *ChemCatChem* **2011**, *3*, 490–511. [CrossRef]

5. Arregi, A.; Amutio, M.; Lopez, G.; Bilbao, J.; Olazar, M. Evaluation of thermochemical routes for hydrogen production from biomass: A review. *Energy Convers. Manag.* **2018**, *165*, 696–719. [CrossRef]

6. Chattahathan, S.A.; Adhikari, A.; Abdoulmoumine, N. A review on current status of hydrogen production from bio-oil. *Renew. Sustain. Energy Rev.* **2012**, *16*, 2366–2372. [CrossRef]

7. Zhang, Y.; Brown, T.R.; Hu, G.; Brown, R.C. Comparative techno-economic analysis of biohydrogen production via bio-oil gasification and bio-oil reforming. *Biomass Bioenergy* **2013**, *51*, 99–108. [CrossRef]

8. Chen, J.; Sun, J.; Wang, Y. Catalysts for steam reforming of bio-oil: A review. *Ind. Eng. Chem. Res.* **2016**, *56*, 4627–4637. [CrossRef]

9. Meier, D.; van de Beld, B.; Bridgwater, A.V.; Elliott, D.C.; Oasmaa, A.; Preto, F. State-of-the-art of fast pyrolysis in IEA bioenergy member countries. *Renew. Sustain. Energy Rev.* **2013**, *20*, 619–641. [CrossRef]

10. Oasmaa, A.; Fonts, I.; Pelaez-Samaniego, M.R.; Garcia-Perez, M.E.; Garcia-Perez, M. Pyrolysis oil multiphase behavior and phase stability: A review. *Energy Fuels* **2016**, *30*, 6179–6200. [CrossRef]

11. Fermoso, J.; Pizarro, P.; Coronado, J.M.; Serrano, D.P. Advanced biofuels production by upgrading of pyrolysis bio-oil. *WIREs Energy Environ.* **2017**, *6*, e245. [CrossRef]

12. Valle, B.; Remiro, A.; Garcia-Gomez, N.; Gayubo, A.G.; Bilbao, J. Recent research progress on bio-oil conversion into bio-fuels and raw chemicals: A review. *J. Chem. Technol. Biotechnol.* **2018**, in press. [CrossRef]

13. Chen, G.; Tao, J.; Liu, C.; Yan, B.; Li, W.; Li, X. Hydrogen production via acetic acid steam reforming: A critical review on catalysts. *Renew. Sustain. Energy Rev.* **2107**, *79*, 1091–1098. [CrossRef]

14. Nabgan, W.; Abdullah, T.A.T.; Mat, R.; Nabgan, B.; Gambo, Y.; Ibrahim, M.; Ahmad, A.; Jalil, A.A.; Triwahyono, S.; Saeh, I. Renewable hydrogen production from bio-oil derivative via catalytic steam reforming: An overview. *Renew. Sustain. Energy Rev.* **2017**, *79*, 347–357. [CrossRef]

15. Remiro, A.; Arandia, A.; Bilbao, J.; Gayubo, A.G. Comparison of Ni based and Rh based catalyst performance in the oxidative steam reforming of raw bio-oil. *Energy Fuels* **2017**, *31*, 7147–7156. [CrossRef]

16. Fierro, V.; Akdim, O.; Provendier, H.; Mirodatos, C. Ethanol oxidative steam reforming over Ni-based catalysts. *J. Power Sources* **2005**, *145*, 659–666. [CrossRef]

17. Graschinsky, C.; Lupiano-Contreras, J.; Amadeo, N.; Laborde, M. Ethanol oxidative steam reforming over $Rh(1\%)MgAl_2O_4Al_2O_3$ catalyst. *Ind. Eng. Chem. Res.* **2014**, *53*, 15348–15356. [CrossRef]

18. Skoplyak, O.; Barteau, M.A.; Chen, J.G. Comparison of H_2 production from ethanol and ethylene glycol on M/Pt(111) (M = Ni, Fe, Ti) bimetallic surfaces. *Catal. Today* **2009**, *147*, 150–157. [CrossRef]

19. Czernik, S.; French, R. Distributed production of hydrogen by auto-thermal reforming of fast pyrolysis bio-oil. *Int. J. Hydrogen Energy* **2014**, *39*, 744–750. [CrossRef]

20. Paasikallio, V.; Azhari, A.; Kihlman, J.; Simell, P.; Lehtonen, J. Oxidative steam reforming of pyrolysis oil aqueous fraction with zirconia pre-conversion catalyst. *Int. J. Hydrogen Energy* **2015**, *40*, 12088–12096. [CrossRef]

21. Remiro, A.; Arandia, A.; Oar-Arteta, L.; Bilbao, J.; Gayubo, A.G. Stability of a Rh/CeO_2-ZrO_2 catalyst in the oxidative steam reforming of raw bio-oil. *Energy Fuels* **2018**, *32*, 3588–3598. [CrossRef]

22. Arandia, A. Catalyst and Conditions in the Oxidative Steam Reforming of Bio-Oil for Stable H_2 Production. Ph.D. Thesis, University of the Basque Country, Bilbao, Spain, 2018.

23. Politano, A.; Chiarello, G. Vibrational investigation of catalyst surface: Change of the adsorption site of CO molecules upon coadsorption. *J. Phys. Chem. C* **2011**, *115*, 13541–13553. [CrossRef]

24. Remiro, A.; Valle, B.; Aguayo, A.T.; Bilbao, J.; Gayubo, A.G. Steam reforming of raw bio-oil in a fluidized bed reactor with prior separation of pyrolytic lignin. *Energy Fuels* **2013**, *27*, 7549–7559. [CrossRef]

25. Valle, B.; Aramburu, B.; Remiro, A.; Bilbao, J.; Gayubo, A.G. Effect of calcination/reduction conditions of Ni/La_2O_3-Al_2O_3 catalyst on its activity and stability for hydrogen production by steam reforming of raw bio-oil/ethanol. *Appl. Catal. B Environ.* **2014**, *147*, 402–410. [CrossRef]

26. Valle, B.; Aramburu, B.; Benito, P.L.; Bilbao, J.; Gayubo, A.G. Biomass to hydrogen-rich gas via steam reforming of raw bio-oil over Ni/La_2O_3-αAl_2O_3 catalyst: Effect of space-time and steam-to-carbon ratio. *Fuel* **2018**, *216*, 445–455. [CrossRef]

27. Valle, B.; Aramburu, B.; Olazar, M.; Bilbao, J.; Gayubo, A.G. Steam reforming of raw bio-oil over Ni/La_2O_3-αAl_2O_3: Influence of temperature on product yields and catalyst deactivation. *Fuel* **2018**, *216*, 463–474. [CrossRef]

28. Liao, X.; Zhang, Y.; Hill, M.; Xia, X.; Zhao, Y.; Jiang, Z. Highly efficient Ni/CeO_2 catalyst for the liquid phase hydrogenation of maleic anhydride. *Appl. Catal. A Gen.* **2014**, *488*, 256–264. [CrossRef]

29. Biswas, P.; Kunzru, D. Steam reforming of ethanol for production of hydrogen over Ni/CeO_2-ZrO_2 catalyst: Effect of support and metal loading. *Int. J. Hydrogen Energy* **2007**, *32*, 969–980. [CrossRef]

30. Ebiad, M.A.; El-Hafiz, D.R.A.; Elsalamony, R.A.; Mohamed, L.S. Ni supported high surface area CeO_2-ZrO_2 catalysts for hydrogen production from ethanol steam reforming. *RSC Adv.* **2012**, *2*, 8145–8156. [CrossRef]

31. Garbarino, G.; Laggazo, A.; Riani, P.; Busca, G. Steam reforming of ethanol-phenol mixture on Ni/Al_2O_3: Effect of Ni loading and sulphur deactivation. *Appl. Catal. B Environ.* **2013**, *129*, 460–472. [CrossRef]

32. Rida, K.; Peña, M.A.; Sastre, E.; Martínez-Arias, A. Effect of calcination temperature on structural properties and catalytic activity in oxidation reactions of $LaNiO_3$ perovskite prepared by Pechini method. *J. Rare Earths* **2012**, *30*, 210–216. [CrossRef]

33. Singh, S.; Zubenko, D.; Rosen, B.A. Influence of $LaNiO_3$ shape on its solid-phase crystallization into coke-free reforming catalysts. *ACS Catal.* **2016**, *6*, 4199–4205. [CrossRef]

34. Silva, T.F.; Dias, J.A.C.; Maciel, C.G.; Assaf, J.M. Ni/Al_2O_3 catalysts: Effects of the promoters Ce, La and Zr on the methane steam and oxidative reforming reactions. *Catal. Sci. Technol.* **2013**, *3*, 635–643. [CrossRef]

35. Ding, M.Y.; Tu, J.y.; Wang, T.J.; Ma, L.L.; Wang, C.G.; Chen, L.G. Bio-syngas methanation towards synthetic natural gas (SNG) over highly active Al_2O_3–CeO_2 supported Ni catalyst. *Fuel Process. Technol.* **2015**, *134*, 480–486. [CrossRef]

36. Khateria, S.; Gupta, A.; Deo, G.; Kunzru, D. Effect of calcination temperature on stability and activity of $Ni/MgAl_2O_4$ catalyst for steam reforming of methane at high pressure condition. *Int. J. Hydrogen Energy* **2016**, *41*, 14123–14132. [CrossRef]

37. Tada, S.; Shimizu, T.; Kameyama, H.; Haneda, T.; Kikuchi, R. Ni/CeO_2 catalysts with high CO_2 methanation activity and high CH_4 selectivity at low temperatures. *Int. J. Hydrogen Energy* **2012**, *37*, 5527–5531. [CrossRef]

38. Holgado, J.P.; Alvarez, R.; Munuera, G. Study of CeO_2 XPS spectra by factor analysis: Reduction of CeO_2. *Appl. Surf. Sci.* **2000**, *161*, 301–315. [CrossRef]

39. Gonzalez-Delacruz, V.M.; Ternero, F.; Pereñiguez, R.; Caballero, A.; Holgado, J.P. Study of nanostructured Ni/CeO_2 catalysts prepared by combustion synthesis in dry reforming of methane. *Appl. Catal. A Gen.* **2010**, *384*, 1–9. [CrossRef]

40. Pengpanich, S.; Meeyoo, V.; Rirksomboon, T. Methane partial oxidation over Ni/CeO_2-ZrO_2 mixed oxide solid solution catalysts. *Catal. Today* **2004**, *93–95*, 95–105. [CrossRef]

41. Roh, H.S.; Koo, K.Y.; Yoon, W.L. Combined reforming of methane over co-precipitated Ni-CeO_2, Ni-ZrO_2 and Ni-$Ce_{0.8}Zr_{0.2}O_2$ catalysts to produce synthesis gas for gas to liquid (GTL) process. *Catal. Today* **2009**, *146*, 71–75. [CrossRef]

42. Guo, C.; Zhang, J.; Zhang, X. Comparative study of $LaNiO_3$ and La_2NiO_4 catalysts for partial oxidation of methane. *React. Kinet. Catal. Lett.* **2008**, *95*, 89–97. [CrossRef]

43. Maneerung, T.; Hidajat, K.; Kawi, S. $LaNiO_3$ perovskite catalyst precursor for rapid decomposition of methane: Influence of temperature and presence of H_2 in feed stream. *Catal. Today* **2011**, *171*, 24–35. [CrossRef]

44. Lin, K.H.; Wang, C.B.; Chien, S.H. Catalytic performance of steam reforming of ethanol at low temperature over LaNiO$_3$ perovskite. *Int. J. Hydrogen Energy* **2013**, *38*, 3226–3232. [CrossRef]

45. Moradi, G.R.; Rahmanzadeh, M.; Khosravian, F. The effects of partial substitution of Ni by Zn in LaNiO$_3$ perovskite catalyst for methane dry reforming. *J. CO$_2$ Util.* **2014**, *6*, 7–11. [CrossRef]

46. Liu, B.S.; Au, C.T. Carbon deposition and catalyst stability over La$_2$NiO$_4$/γ-Al$_2$O$_3$ during CO$_2$ reforming of methane to syngas. *Appl. Catal. A Gen.* **2003**, *244*, 181–195. [CrossRef]

47. Li, P.; Yu, B.; Li, J.; Yao, X.; Zhao, Y.; Li, Y. A single layer solid oxide fuel cell composed of La$_2$NiO$_4$ and doped ceria-carbonate with H$_2$ and methanol as fuels. *Int. J. Hydrogen Energy* **2016**, *41*, 9059–9065. [CrossRef]

48. Fontaine, M.L.; Laberty-Robert, C.; Ansart, F.; Tailhades, P. Elaboration and characterization of La$_2$NiO$_{4+\delta}$ powders and thin films via a modified sol–gel process. *J. Solid State Chem.* **2004**, *177*, 1471–1479. [CrossRef]

49. Gallego, G.S.; Mondragón, F.; Tatibouët, J.M.; Barrault, J.; Batiot-Dupeyrat, C. Carbon dioxide reforming of methane over La$_2$NiO$_4$ as catalyst precursor-Characterization of carbon deposition. *Catal. Today* **2008**, *133–135*, 200–209. [CrossRef]

50. Benrabaa, R.; Barama, A.; Boukhlouf, H.; Guerrero-Caballero, J.; Rubbens, A.; Bordes-Richard, E.; Löfberg, A.; Vannier, R.N. Physico-chemical properties and syngas production via dry reforming of methane over NiAl$_2$O$_4$ catalyst. *Int. J. Hydrogen Energy* **2017**, *42*, 12989–12996. [CrossRef]

51. Diagne, C.; Idriss, H.; Kiennemann, A. Hydrogen production by ethanol reforming over Rh/CeO$_2$-ZrO$_2$ catalysts. *Catal. Commun.* **2002**, *3*, 565–571. [CrossRef]

52. Varez, A.; Garcia-Gonzalez, E.; Sanz, J. Cation miscibility in CeO$_2$-ZrO$_2$ oxides with fluorite structure. A combined TEM, SAED and XRD Rietveld analysis. *J. Mater. Chem.* **2006**, *16*, 4249–4256. [CrossRef]

53. Reddy, L.H.; Reddy, G.K.; Devaiah, D.; Reddy, B.M. A rapid microwave-assisted solution combustion synthesis of CuO promoted CeO$_2$-M$_x$O$_y$ (M = Zr, La, Pr and Sm) catalysts for CO oxidation. *Appl Catal A Gen.* **2012**, *445−446*, 297–305. [CrossRef]

54. Li, J.; Liu, X.; Zhan, W.; Guo, Y.; Guo, Y.; Lu, G. Preparation of high oxygen storage capacity and thermally stable ceria–zirconia solid solution. *Catal. Sci. Technol.* **2016**, *6*, 897–907. [CrossRef]

55. Ochoa, A.; Barbarias, I.; Artetxe, M.; Gayubo, A.G.; Olazar, M.; Bilbo, J.; Castaño, P. Deactivation dynamics of a Ni supported catalyst during the steam reforming of volatiles from waste polyethylene pyrolysis. *Appl. Catal. B Environ.* **2017**, *209*, 554–565. [CrossRef]

56. Dong, X.; Wu, Z.; Chang, X.; Jin, W.; Xu, N. One-step synthesis and characterization of La$_2$NiO$_{4+\delta}$ mixed-conductive oxide for oxygen permeation. *Ind. Eng. Chem. Res.* **2007**, *46*, 6910–6915. [CrossRef]

57. Qin, H.; Guo, C.; Wu, Y.; Zhang, J. Effect of La$_2$O$_3$ promoter on NiO/Al$_2$O$_3$ catalyst in CO methanation. *Korean J. Chem. Eng.* **2014**, *31*, 1168–1173. [CrossRef]

58. Si, J.; Liu, G.; Liu, J.; Zhao, L.; Li, S.; Guan, Y.; Liu, Y. Ni nanoparticles highly dispersed on ZrO$_2$ and modified with La$_2$O$_3$ for CO methanation. *RSC Adv.* **2016**, *6*, 12699–12707. [CrossRef]

59. Arora, S.; Prasad, R. An Overview on dry reforming of methane: Strategies to reduce carbonaceous deactivation of catalysts. *RSC Adv.* **2016**, *6*, 108668–108688.

60. Li, D.; Li, X.; Gong, J. Catalytic reforming of oxygenates: State of the art and future prospects. *Chem. Rev.* **2016**, *116*, 11529–11653. [CrossRef] [PubMed]

61. Ochoa, A.; Aramburu, B.; Valle, B.; Resasco, D.E.; Bilbao, J.; Gayubo, A.G.; Castaño, P. Role of oxygenates and effect of operating conditions in the deactivation of a Ni supported catalyst during the steam reforming of bio-oil. *Green Chem.* **2017**, *19*, 4315–4333. [CrossRef]

62. Guo, Y.; Zou, J.; Shi, X.; Rukundo, P.; Wang, Z.J. A Ni/CeO$_2$-CDC-SiC catalyst with improved coke resistance in CO$_2$ reforming of methane. *ACS Sustain. Chem. Eng.* **2017**, *5*, 2330–2338. [CrossRef]

63. Davidian, T.; Guilhaume, N.; Iojoiu, E.; Provendier, H.; Mirodatos, C. Hydrogen production from crude pyrolysis oil by a sequential catalytic process. *Appl. Catal. B Environ.* **2007**, *73*, 116–127. [CrossRef]

64. Wu, C.; Liu, R. Sustainable hydrogen production from steam reforming of bio-oil model compound based on carbon deposition/elimination. *Int. J. Hydrogen Energy* **2011**, *36*, 2860–2868. [CrossRef]

65. Lónyi, F.; Valyon, J.; Someus, E.; Hancsók, J. Steam reforming of bio-oil from pyrolysis of MBM over particulate and monolith supported Ni/γ-Al$_2$O$_3$ catalysts. *Fuel* **2013**, *112*, 23–30. [CrossRef]

66. Remiro, A.; Arandia, A.; Oar-Arteta, L.; Bilbao, J.; Gayubo, A.G. Regeneration of NiAl$_2$O$_4$ spinel type catalysts used in the reforming of raw bio-oil. *Appl. Catal. B Environ.* **2018**, *237*, 353–365. [CrossRef]

67. Alberton, A.L.; Souza, M.; Schmal, M. Carbon formation and its influence on ethanol steam reforming over Ni/Al$_2$O$_3$ catalysts. *Catal. Today* **2007**, *123*, 257–264. [CrossRef]

68. Gómez-Gualdrón, D.; Balbuena, P. Characterization of carbon atomistic pathways during single-walled carbon nanotube growth on supported metal nanoparticles. *Carbon* **2013**, *57*, 298–309. [CrossRef]

69. Shamskar, F.R.; Rezaei, M.; Meshkani, F. The influence of Ni loading on the activity and coke formation of ultrasound-assisted co-precipated $Ni-Al_2O_3$ nanocatalyst in dry reforming of methane. *Int. J. Hydrogen Energy* **2017**, *42*, 4155–4164. [CrossRef]

70. Tanksale, A.; Zhou, C.H.; Beltramini, J.N.; Lu, G.Q. Hydrogen production by aqueous phase reforming of sorbitol using bimetallic Ni–Pt catalysts: Metal support interaction. *J. Incl. Phenom. Macrocycl. Chem.* **2009**, *65*, 83–88. [CrossRef]

71. Chen, L.; Choong, C.K.S.; Zhong, Z.; Huanf, L.; Wang, Z.; Lin, J. Support and alloy effects on activity and product selectivity for ethanol steam reforming over supported nickel cobalt catalysts. *Int. J. Hydrogen Energy* **2012**, *37*, 16321–16332. [CrossRef]

72. Zhang, R.J.; Xia, G.F.; Li, M.F.; Wu, Y.; Nie, H.; Li, D.D. Effect of support on the performance of Ni-based catalyst in methane dry reforming. *J. Fuel Chem. Technol.* **2015**, *43*, 1359–1365. [CrossRef]

73. Ochoa, A.; Arregui, A.; Amutio, M.; Gayubo, A.G.; Olazar, M.; Bilbao, J.; Castaño, P. Coking and sintering progress of a Ni supported catalyst in the steam reforming of biomass pyrolysis volatiles. *Appl. Catal. B Environ.* **2018**, *233*, 289–300. [CrossRef]

74. Valle, B.; Remiro, A.; Aguayo, A.T.; Bilbao, J.; Gayubo, A.G. Catalysts of $Ni/\alpha-Al_2O_3$ and $Ni/La_2O_3-\alpha Al_2O_3$ for hydrogen production by steam reforming of bio-oil aqueous fraction with pyrolytic lignin retention. *Int. J. Hydrogen Energy* **2013**, *38*, 1307–1318. [CrossRef]

75. Roh, H.S.; Potdar, H.S.; Jun, K.W. Carbon dioxide reforming of methane over co-precipitated $Ni-CeO_2$, $Ni-ZrO_2$ and $Ni-Ce-ZrO_2$ catalysts. *Catal. Today* **2004**, *93–95*, 39–44. [CrossRef]

76. Arandia, A.; Remiro, A.; Valle, B.; Bilbao, J.; Gayubo, A.G. Operating strategies for the oxidative steam reforming (OSR) of raw bio-oil in a continuous two-step system. *Chem. Eng. Trans.* **2017**, *57*, 217–222.